FSTL1 secreted by activated fibroblasts promotes hepatocellular carcinoma metastasis and stemness

Jia Jian Loh[1], Tsz Wai Li[1], Lei Zhou[1], Tin Lok Wong[1], Xue Liu[4], Victor WS Ma[1], Chung Mau Lo[2,5,6], Kwan Man[2,5,6], Terence K Lee[3], Wen Ning[4], Man Tong[1,5#], Stephanie Ma[1,5,6#]

[1]School of Biomedical Sciences, Li Ka Shing Faculty of Medicine, The University of Hong Kong;

[2]Department of Surgery, Li Ka Shing Faculty of Medicine, The University of Hong Kong;

[3]Department of Applied Biology and Chemical Technology, The Hong Kong Polytechnic University;

[4]State Key Laboratory of Medicinal Chemical Biology, College of Life Sciences, Nankai University;

[5]State Key Laboratory of Liver Research, The University of Hong Kong;

[6]The University of Hong Kong – Shenzhen Hospital

[#]**Correspondence to** Dr. Stephanie Ma, PhD, School of Biomedical Sciences, Li Ka Shing Faculty of Medicine, The University of Hong Kong. E-mail: stefma@hku.hk. Tel: +852 3917 9238 or Dr. Man Tong, PhD, School of Biomedical Sciences, Li Ka Shing Faculty of Medicine, The University of Hong Kong. E-mail: caroltm@hku.hk. Tel: +852 3917 9424.

Keywords: FSTL1; cancer-associated fibroblasts; tumor microenvironment; TLR4; cancer stemness; tumor-initiating; drug resistance; antibody therapy

Declaration of interests: The authors declare no competing interests.

The following publication Jia-Jian Loh, Tsz-Wai Li, Lei Zhou, Tin-Lok Wong, Xue Liu, Victor W.S. Ma, Chung-Mau Lo, Kwan Man, Terence K. Lee, Wen Ning, Man Tong, Stephanie Ma; FSTL1 Secreted by Activated Fibroblasts Promotes Hepatocellular Carcinoma Metastasis and Stemness. Cancer Res 15 November 2021; 81 (22): 5692–5705 is available at https://dx.doi.org/10.1158/0008-5472.CAN-20-4226.

ABSTRACT

The tumor microenvironment plays a critical role in maintaining the immature phenotype of tumor-initiating cells (TIC) to promote cancer. Hepatocellular carcinoma (HCC) is a unique disease in that it develops in the setting of fibrosis and cirrhosis. This pathological state commonly shows an enrichment of stromal myofibroblasts, which constitute the bulk of the tumor microenvironment and contribute to disease progression. Follistatin-like 1 (FSTL1) has been widely reported as a pro-inflammatory mediator in different fibrosis-related and inflammatory diseases. Here we show FSTL1 expression to be closely correlated with activated fibroblasts and to be elevated in regenerative, fibrotic, and disease liver states in various mouse models. Consistently, FSTL1 lineage cells gave rise to myofibroblasts in a CCL_4-induced hepatic fibrosis mouse model. Clinically, high FSTL1 in FAP+ fibroblasts were significantly correlated with more advanced tumors in HCC patients. Although FSTL1 was expressed in primary fibroblasts derived from HCC patients, it was barely detectable in HCC cell lines. Functional investigations revealed that treatment of HCC cells and patient-derived 3D organoids with recombinant FSTL1 or with conditioned medium collected from hepatic stellate cells or from cells overexpressing FSTL1 could promote HCC growth and metastasis. FSTL1 bound to TLR4 receptor, resulting in activation of AKT/mTOR/4EBP1 signaling. In a pre-clinical mouse model, blockade of FSTL1 mitigated HCC malignancy and metastasis, sensitized HCC tumors to sorafenib, prolonged survival, and eradicated the TIC subset. Collectively, these data suggest that FSTL1 may serve as an important novel diagnostic/prognostic biomarker and therapeutic target in HCC.

STATEMENT OF SIGNIFICANCE

This study shows that FSTL1 secreted by activated fibroblasts in the liver microenvironment augments hepatocellular carcinoma malignancy, providing a potential new strategy to improve treatment of this aggressive disease.

INTRODUCTION

Globally, hepatocellular carcinoma (HCC) is the sixth most common cancer and third deadliest cancer, causing more than 800,000 new cases and approximately 800,000 deaths in 2018 (1). The presence of liver fibrosis, a consequence of continuous repair and damage, is a prominent risk factor of HCC development with 80-90% of all cases observed to be accompanied by a fibrotic or cirrhotic liver (2). HCC can be illustrated as a multi-step disease in which a normal liver develops cirrhosis, followed by the manifestation of dysplastic features, ultimately neoplastic transformation into HCC. Depending on the demographical and etiological factors such as hepatitis B and C viral infection, 5-30% of the patients with cirrhotic liver develop HCC in the next five years (3). Accordingly, patients with more advanced cirrhosis have greater risk of developing HCC. Together, a fibrotic liver that is regularly undergoing repair may offer a permissive pre-malignant microenvironment and tumor microenvironment (TME) for hepatocytes regeneration and cancer cells progression, respectively (4). Myofibroblast, an activated form of fibroblast, plays vital role in tissue repair and fibrosis, partly by producing growth factors crucial for growth (4). A fibrotic or cirrhotic liver is enriched for pro-inflammatory factors secreted from activated fibroblasts and immune cells to promote growth upon injury (4,5), thereby providing the opportunity for cancer cells to exploit this recovery machinery for progression.

To date, merely two categories of FDA-approved drugs are in clinical practice for advanced HCC, namely multi-kinase and immune checkpoint inhibitors. Among the multi-kinase inhibitors, sorafenib is commonly administered as first-line therapy (6). However, sorafenib can only extend the median survival for approximately 3 months (7), thereby highlighting the urgent need to develop novel treatment for advanced HCC. Tumor-initiating cells (TICs), alternatively named cancer stem cells (CSCs), are categorized by their enhanced self-renewal properties which can confer resistance to therapy by regeneration of the depleted tumor (8). TICs rely heavily on the TME to maintain its stemness (9). Cancer-associated fibroblast (CAF), a component of the stromal fraction in the TME, can contribute to the stemness of TICs by secreting growth factors, such as CCL2 and HGF to upregulate Notch and Wnt stemness signaling (10-12). CAFs have been shown to promote chemoresistance and maintaining cancer stemness by the secretion of IL-6 (13). CAF-derived factors are also shown to promote cancer cell invasion and migration (14-16). However, the mechanism in which a highly

inflammatory pre-malignant microenvironment during liver fibrosis translates to a TME that contributes to malignant properties of HCC remains largely unknown.

FSTL1 is a pro-inflammatory factor which is found to be upregulated during inflammation in tissue such as the joint, lung and heart (17-19). FSTL1 has been reported to promote malignant properties in various cancers, such as breast, esophageal and colon cancers (20-22). Considering the known role of FSTL1 in inflammation and most HCCs developed in a cirrhosis background, the role of FSTL1 in mediating HCC warrants further investigation. Here, we identified Fstl1 to be upregulated in regenerative, fibrotic and disease states using different mouse models of the liver. Fstl1 lineage cells gave rise to myofibroblasts in a CCL_4-induced hepatic fibrosis mouse model. We further demonstrated that FSTL1 is predominantly secreted from the stromal cells rather than liver cancer cells. *In vitro* and *in vivo* functional assays showed FSLTL1 augments the stemness, proliferation, metastasis and therapy resistance properties of liver cancer cells. Importantly, neutralizing antibody attenuates FSTL1-mediated malignancy. Mechanistically, FSTL1 binds to TLR4 receptor on HCC cells to activate oncogenic effects through a deregulated AKT/mTOR/MYC signaling cascade. Pre-clinical immunocompetent mouse model demonstrated the treatment of HCC tumors with a specific FSTL1 neutralizing monoclonal antibody (nAb) sensitized it to sorafenib, prolonged survival and eradicated the liver tumor-initiating cell subset. Together, we unraveled FSTL1's potential as a novel prognostic biomarker and therapeutic target in HCC.

MATERIALS AND METHODS

Cell lines and fibroblasts. Hepatic stellate cell line hTERT-HSC was obtained as a gift from David Brenner of UC San Diego (23). CHO-K1 cell line and HCC cell lines Hep3B, HepG2 were purchased from American Type Culture Collection (ATCC). HCC cell line PLC8024 was obtained from the Institute of Virology of the Chinese Academy of Sciences. HCC cell line Huh7 was purchased from the JCRB Cell Bank. HCC cell line SNU878 was purchased from the Korean Cell Line Bank. HCC cell lines MHCC97L and MHCC97H were obtained from the Liver Cancer Institute, Fudan University. MIHA was provided by Dr. JR Chowdhury of Albert Einstein College of Medicine. Normal liver fibroblast line was purchased from iBiologics. Cell lines used in this study were regularly authenticated by morphological observation and AuthentiFiler STR (Invitrogen) and tested for absence of Mycoplasma contamination. Experiments were performed within 30 passages after cell thawing.

HCC patient-derived organoids. For patient-derived organoid cultures, cells were isolated and cultured as previously described (24-26). HCC tissue used for organoid establishment of HCC patient-derived organoid HK-HCC P1 was obtained from HCC patient undergoing hepatectomy or liver transplantation at Queen Mary Hospital, Hong Kong, with written informed consent obtained from all patients and protocol approved by the Institutional Review Board of the University of Hong Kong/Hospital Authority Hong Kong West Cluster. Samples were collected from patients who had not received any previous local or systemic treatment prior to operation.

Clinical samples. Frozen primary human HCC and adjacent non-tumor liver tissue samples were obtained from HCC patients undergoing hepatectomy at Queen Mary Hospital, Hong Kong, with written informed consent obtained from all patients and protocol approved by the Institutional Review Board of the University of Hong Kong / Hospital Authority Hong Kong West Cluster. Samples were collected from patients who had not received any previous local or systemic treatment prior to operation.

CAF score. CAF score was computed as described in a previous study (27). Liver cancer data was downloaded from https://xena.ucsc.edu/. Liver CAF score signature was the mean of genes specific to

liver CAF, as determined by previous study (28). The correlation between FSTL1 and CAF score were analyzed using GraphPad Prism 6.0.

Animal study approval. Animal research ethics was approved by and performed in accordance with the Committee of the Use of Live Animals in Teaching and Research at The University of Hong Kong and the Animals (Control of Experiments) Ordinance of Hong Kong or the Animal Care and Use Committee at Nankai University.

Liver regeneration mouse model by partial hepatectomy. Surgery was performed as previously described (29). Briefly, C57BL/6 mice were anesthetized with 80 mg/kg ketamine and 10 mg/kg xylazine (i.p.). The left lobe and the median lobe were ligated separately and resected to achieve 2/3 hepatectomy. Animals were sacrificed on days 1.5, 3 or 7 after surgery.

DEN+CCL_4 fibrosis-induced HCC mouse model. Mice were treated with DEN (i.p., 1mg/kg) at the age of 14 days. Starting at 8 weeks of age, CCl_4 (i.p., 0.2ml/kg) was administered twice weekly for 12 to 16 weeks (30). Tumors started to grow at the age of ~21 weeks, and the humane endpoint of this model was at the age of 24 weeks. Animals were sacrificed at weeks 8, 16, 18, 20, 22, 23 and 24.

Hydrodynamic tail vein NRAS+AKT HCC mouse model. 6-to-8-week old male wild-type C57BL/6 mice were used and the procedure was performed as previously described (31-32). In brief, 20μg of plasmids encoding human AKT1 (myristylated AKT1 or myr-AKT1) and human neuroblastoma Ras viral oncogene homolog (N-RasV12) along with sleeping beauty (SB) transposase in a ratio of 25:1 were diluted in 2ml saline (0.9% NaCl), filtered through 0.22μm filter and injected into the lateral tail vein of C57BL/6 mice in 5-7s. The constructs used in this study showed long term expression of genes via hydrodynamic injection (32). Three weeks post hydrodynamic tail vein injection of proto-oncogenes and SB transposase, mice were separated into four groups and administered with (i) DMSO + IgG or (ii) sorafenib + IgG or (iii) DMSO + FSTL1 nAb or (iv) sorafenib + FSTL1 nAb. Sorafenib was administered at 30mg/kg/day. FSTL1 nAb was administered at a concentration of 2.5mg/kg every 3 days.

***Fstl1-CreERT2* mouse model, CCL_4 induced liver injury and tamoxifen administration.** *Fstl1-CreERT2* knock in mice were generated in Model Animal Research Center of Nanjing University. *Rosa-mT-mG (B6.129(Cg)-Gt(ROSA)26Sortm4 (ACTBtdTomato-EGFP)LuoJ* mice were purchased from Model Animal Research center of Nanjing University (stock number: J007676). *Fstl1-CreERT2; Rosa26-mT-mG* mouse line was obtained by crossing *Fstl1-CreERT2* mice with lineage reporter *Rosa26-mT-mG* mice. The genotypes of the mice were determined by PCR as previously described (33). A tamoxifen stock solution of 10mg/ml was produced by dissolving tamoxifen powder in corn oil. To examine recombination in the liver, mice received five doses of tamoxifen by intraperitoneal injection before or after CCL_4 treatment and were sacrificed at indicated time for sectioning and analysis.

Immunofluorescence on live cells. Cells were fixed with 4% paraformaldehyde, permeabilized with 0.1% Triton X (Sigma-Aldrich), blocked with 5% bovine serum albumin and incubated with FSTL1 (1:200, abcam, ab71548), αSMA (1:400, abcam, ab21027), FAP (1:100, abcam, ab28244), CD31 (1:100, Invitrogen, MA3100), pan-cytokeratin (1:500, abcam, ab7753), followed by Alexa-Fluor conjugated secondary antibody (1:500, Life Technologies). Immunofluorescence on Fstl1 lineage model was performed as previously reported (33). Antibodies used were GFP (1:1000, abcam, ab13970) and αSMA (1:500, Santa Cruz, sc-32251). For colocalization of TLR4 and FSTL1, MHCC97L cells were first treated with 10ng/mL of recombinant human FSTL1 (R&D Systems) and incubated for 8hrs. Cells were then fixed, permeabilized and blocked as indicated above, and incubated with FSTL1 (1:100, abcam, ab71548) and TLR4 (1:100, Novus Biologicals, NB100-56566), followed by Alexa-Fluor conjugated secondary antibody (1:500, Life Technologies). Cells were counterstained with anti-fade DAPI (Invitrogen), visualized by fluorescent confocal microscope (Carl Zeiss LSM 780) and analyzed using ZEN 2 (blue edition) software.

Immunofluorescence on paraffin-embedded tissues. After dewaxing and rehydration of the paraffin-embedded sections, the antigen-retrieval was conducted using Envision Flex Target Retrieval Solution of high pH (DAKO). For FSTL1 and αSMA staining, the sections were blocked with Opal Antibody Diluent/Block (AKOYA), followed by incubation with FSTL1 (1:100, abcam, ab71548) for 1hr at room temperature. Signal was detected by incubating Opal Polymer HRP, Mouse plus Rabbit (AKOYA) for 30 minutes, followed by Opal 570 Reagent (AKOYA). Another round of antigen retrieval and antibody

stripping were conducted before incubating with αSMA (1:100, abcam, ab5694) for 1hr at room temperature. Signal was detected by incubating Opal Polymer HRP, Mouse plus Rabbit (AKOYA) for 30 minutes, followed by Opal 520 Reagent (AKOYA). DAPI (AKOYA) was used to counterstain the nuclei. p-AKT and pan-CK staining was done as described above, with p-AKT (Ser473) (1:200, Cell Signaling, 4060) and pan-CK (1:200, abcam, ab7753) stained with Opal 570 and Opal 520 Reagent (AKOYA), respectively. The sections were imaged using Vectra Polaris imaging system (Perkin Elmer). Analysis to segment and quantify the cells based on their immunostaining were performed using inForm versions 2.2 (Akoya Biosciences).

RNA extraction, cDNA synthesis and quantitative real-time PCR (qPCR). Total RNA was extracted using RNA-IsoPlus (Takara) and cDNA was synthesized by PrimeScript RT Master Mix (Takara). qPCR was performed with EvaGreen qPCR Master Mix (ABM) and primers listed in **Supplemental Table S1** on a LightCycler 480 II analyzer (Roche) with data analyzed using the LightCycler 480 II software (Roche). Relative expression differences were calculated using the $2^{-\Delta\Delta Ct}$ method.

Lentiviral production and cell transduction. *CD14*-specific shRNA expression vectors (NM_000591), *DIP2A*-specific shRNA expression vectors (NM_015151), and scrambled shRNA non-target control (NTC) were purchased from Sigma-Aldrich. *TLR4*-specific shRNA expression vectors (NM_138554) were manufactured by IGE Bio. Sequences were packaged using MISSION Lentiviral Packaging Mix (Sigma-Aldrich) and transfected into 293FT cells. Virus-containing supernatants were collected for subsequent transduction to establish cells with CD14, DIP2A or TLR4 stably repressed. Puromycin was used for cell selection. shRNA sequences used are listed in **Supplemental Table S2**.

siRNA transfection. siRNA sequences used are listed in **Supplemental Table S3**. Please see Supplemental File for methods details.

RESULTS

***Fstl1* expression is closely correlated with activated fibroblasts and elevated in regenerative, fibrotic and disease states in various mouse models of the liver.** Atypical fibrotic response is widely associated with increased aggressiveness and poor prognosis in cancers. In HCC, around 90% of cases are associated with fibrosis or cirrhosis, a disease which is characterized by an enrichment of activated fibroblasts due to chronic inflammation. We initiated the study by looking at fibroblasts in a liver regenerating mouse model induced by 70% partial hepatectomy where hepatocyte proliferation and enhanced expression of activated fibroblasts are commonly observed. We found *Fstl1* to be significantly upregulated during active liver regeneration on day 3 with its expression slightly decreasing towards the end of liver regeneration when the liver is mostly restored on day 7. Notably, expressions of *Fstl1* tightly correlated with *Acta2* mRNA expression, which encodes for αSMA, a major marker of myofibroblasts (**Figure 1A**). Next, to understand the regulatory mechanism of fibroblasts in HCC, we examined *Fstl1* and *Acta2* expression in two HCC mouse models induced either by hydrodynamic tail vein injection (HTVI) of oncogenic plasmids (NRAS+AKT) and sleeping beauty transposase or administration of DEN+CCL_4. Consistently, we found *Fstl1* expression to be greatly enhanced at advanced stages of tumor development (~4-5 weeks for HTVI induced HCC and ~22 weeks for DEN+CCL_4 induced HCC) with its expression closely correlated with *Acta2* levels (**Figure 1B-C**). Expression of Fstl1 and αSMA proteins is also co-localized in the tumor tissue sections of the DEN+CCL_4 mouse model, as demonstrated by immunofluorescence (**Supplemental Figure S1**). Lineage tracing of Fstl1 in a CCL_4 induced liver fibrosis model in *Fstl1-CreERT2;Rosa26-mT-mG* mice found *de novo* (model 1) but not resident (model 2) Fstl1 lineage cells to be labeled with GFP and that *de novo* Fstl1 cells overlap with αSMA fibroblasts, suggesting that Fstl1 expressing myofibroblasts is induced in CCL_4 mediated liver fibrosis (**Figure 1D**).

FSTL1 is preferentially overexpressed in the stromal CAFs in human hepatocellular carcinoma. To understand the role of cancer-associated fibroblasts (CAFs) in hepatocarcinogenesis, we obtained freshly resected non-tumor liver and HCC clinical samples from patients who underwent surgery for HCC removal and isolated non-tumor fibroblasts (NF) and CAF pairs (*n*=3). All isolated fibroblasts displayed a homogenous spindle-shaped fibroblastic morphology that stained positive for both αSMA and fibroblast activation protein (FAP) (**Supplemental Figure S2**). To ensure the established

fibroblasts were free of contaminating HCC, endothelial and epithelial cells, we also examined for expression of the respective markers, alpha-fetoprotein (AFP), CD31 and pan-cytokeratin, which all stained negative (**Supplemental Figure S2**). We then examined the secretory expression levels of FSTL1 in normal liver fibroblasts, hTERT-hepatic stellate cells (HSC), NFs, CAFs and a panel of HCC cell lines. All immortalized normal liver and HCC cells (MIHA, MHCC97L, MHCC97H, SNU878, HepG2, PLC8024, Huh7 and Hep3B) produced no or negligible levels of FSTL1, while normal fibroblasts, hTERT-HSC, NFs and CAFs produced significantly higher amounts (**Figure 1E**). Notably, normal fibroblasts secreted some levels of FSTL1, but all three CAF lines secreted significantly more than their paired NF and normal fibroblast, suggesting that fibroblast and in particular CAFs in the tumor stroma represent a major source of FSTL1. hTERT-HSC also secreted more FSTL1 compared to normal fibroblast (**Figure 1E**). We also found FSTL1 to be significantly associated with an HCC CAF signature as defined by a 12-marker panel comprising expressions of FGF5, CXCL5, IGFL2, MMP1, ADAM32, ADAM18, IGFL1, FGF8, FGF17, FGF19, FGF4 and FGF23 (34) (**Figure 1F**). Consistent with the findings in our mouse models, we found the majority of FSTL1 expressing cells to overlap with those of αSMA in HCC (*n*=4) clinical samples and that FSTL1 is secreted in more abundance in HCC than as compared to its adjacent non-tumor liver (**Figure 1G-H).** Analysis of our data collected in-house as well as in the TCGA LIHC dataset found FSTL1 expression to positively correlate with ACTA2 and FAP, respectively, suggesting FSTL1 to be primarily derived from myofibroblasts/CAFs (**Figure 1I**). To confirm the clinical relevance of FSTL1 expression, we further examined the TCGA LIHC dataset and found high FSTL1 in the FAP+ CAF subset to be significantly correlated with advanced tumor stages in HCC tumor tissues as compared to low FSTL1 in FAP+ CAFs, suggesting the clinical implication of high FSTL1 in CAFs of HCC (**Figure 1J**).

FSTL1 promotes malignant properties in HCC cells *in vitro* and *in vivo*. To investigate the causative relationship between enhanced FSTL1 secretion by CAFs in hepatocarcinogenesis, we overexpressed empty vector control or FSTL1 in CHO-K1 cells, chosen for its high yield and reduced non-specific production of recombinant proteins, and collected empty vector conditioned medium (EV CM) or FSTL1 overexpressing conditioned medium (FSTL1 OE CM), respectively. For subsequent functional studies, MHCC97L cell line was chosen because it does not express any endogenous FSTL1 and for its ability to grow when injected orthotopically in the liver for the study of metastasis. Note that

secretory FSTL1 level in CHO-K1 cells was expressed at physiological level that is comparable to that of CAFs (**Figure 1E**). FSTL1 OE CM enhanced the abilities of MHCC97L HCC cells to proliferate (**Figure 2A**), migrate (**Figure 2B**) and invade (**Figure 2C**). Stem cell-like properties of cancer cells can contribute to cancer relapse due to their ability to self-renew and resist standard therapy. Thus, we also evaluated whether FSTL1 OE CM can alter these properties. Co-culture of FSTL1 OE CM enhanced ability of HCC cells to resist molecular targeted therapy sorafenib as demonstrated by a decrease in number of dead cells measured by Annexin V PI flow cytometry analysis (**Figure 2D**) and also to self-renew with the latter demonstrated by an increase in the frequency of tumor-initiating cells (TICs) in a limiting dilution spheroid formation assay (**Figure 2E**). Consistently, administration of recombinant FSTL1 (rhFSTL1) at a level comparable to that secreted by CAFs (**Figure 1E**) also resulted in similar pro-tumorigenic functional effects (**Figure 2A-E, right panel**). We also extended our study to a more physiological setting, utilizing organotypic *ex vivo* culture of HCC tumor tissues where pathophysiology of the original tumor is better preserved than as compared to cell lines. Note the HCC patient-derived organoid used here is thoroughly characterized at both molecular and phenotypic levels, with comparison made against the original tissue samples (***see Supplemental Information – For Review Only***). Consistently, similar results could be attained when HCC patient-derived organoids were treated with FSTL1 OE CM or rhFSTL1 (**Supplemental Figure S3A-E**).

In line with our findings *in vitro* and *ex vivo*, treatment of MHCC97L cells with FSTL1 OE CM also promoted tumor growth potential *in vivo* in immunocompromised nude mice, as demonstrated by increased proliferative and incidence rates (**Figure 2F**). In a separate experiment, we also implanted MHCC97L HCC cells at limiting dilutions subcutaneously into immunocompromised NOD-SCID mice and administered either EV CM or FSTL1 OE CM to the tumor injection site every 3 days. HCC cells treated with FSTL1 OE CM exhibited a significantly worse tumor-free survival compared with HCC cells treated with EV CM (**Figure 2G**) as well as increased tumor incidence, expedited tumor latency, close to a 5-fold higher frequency of TIC (**Supplemental Table S4**). At end point, HCC tumor cells were harvested from the liver for *ex vivo* limiting dilution spheroid formation assay, where it was demonstrated that the frequency of TIC capable of forming spheres also increased when HCC cells were treated with FSTL1 OE CM (**Figure 2H**). An orthotopic liver metastasis model was also carried out to examine ability of FSTL1 to alter ability of HCC cells to metastasize *in vivo*. And indeed,

MHCC97L HCC cells treated with FSTL1 OE CM displayed a superior ability to metastasize to the lung than as compared to HCC cells treated with EV CM, as supported by stronger bioluminescence signal, bigger liver to body weight ratio (**Figure 2I**) as well as number of metastatic nodules detected in the lung (**Figure 2J**). Collectively, these findings support a key role of secretory FSTL1 in promoting tumorigenicity, self-renewal and metastasis in HCC.

Blockade of FSTL1 by a specific monoclonal neutralizing antibody mitigates HCC malignancy. In light of the above findings, we reasoned that blocking FSTL1 signaling with a neutralizing antibody (nAb) may be therapeutic for HCC. Our co-author Prof. Wen Ning has previously generated a FSTL1 nAb (clone 22B6) with binding affinity, kinetics and neutralization function fully characterized (19). Due to its high similarity (>95%) in gene expression with activated human HSC, hTERT-HSC was used as a model to study the paracrine effect of the stromal fraction on HCC cells (23). Treatment of MHCC97L HCC cells with CM collected from the hepatic stellate cell line hTERT-HSC (23) neutralized by FSTL1 nAb resulted in diminished ability of cells to proliferate (**Figure 3A**), migrate (**Figure 3B**) and invade (**Figure 3C**). Treatment of FSTL1 OE CM with nAb also reversed sensitivity of HCC cells to sorafenib (**Figure 3D**) and reverted TIC frequency of MHCC97L cells to levels comparable to the EV CM + IgG control (**Figure 3E**). Similar effects could also be observed when treatment was done in HCC patient-derived 3D organoids **(Supplemental Figure S4A-D**). Consistently, we were able to see comparable findings when we used the FSTL1 nAb against FSTL1 OE CM, where the neutralizing antibody reverted the functional phenotypes back to the level of EV CM (**Figure 3A-E, right panel**).

Complementary *in vivo* studies were also performed. Proliferative growth of tumors formed with MHCC97L cells treated with FSTL1 OE CM was significantly attenuated in the presence of FSTL1 nAb, with tumor volume and weight returning to a similar level than of tumors formed with MHCC97L cells treated with EV CM (**Figure 4A**). When the same cells were injected at limiting dilutions in immunodeficient NOD-SCID mice, FSTL1 nAb delivery clearly reduced tumor incidence, delayed time needed for successful engraftment and reverted the TIC frequency to a similar level than that of the EV CM + IgG control group in primary implantation. When liver tumors from these primary implantations were harvested for serial transplantation into secondary mouse recipients, a further decrease in tumor incidence and TIC frequency could be observed in the nAb treated group (500 cells

– 2/10; 1000 cells – 2/9; TIC frequency 1:2674) as compared to the control (500 cells – 6/10; 1000 cells – 4/9; TIC frequency 1:1000), suggesting FSTL1 nAb could decrease self-renewal ability and the functional cancer stemness subset of the HCC tumor (**Supplemental Table S5**). FSTL1 nAb could also prolong tumor free survival in both primary and secondary implantations of the mouse model (**Figure 4B**); and led to further inhibition of tumor growth in secondary transplantations (**Figure 4C**). *Ex vivo* limiting dilution spheroid formation assay with liver tumor cells harvested from primary implantations also yielded similar results as those of *in vivo* secondary implantations (**Figure 4D**) further confirming our observations. Similar inhibitory effects could also be extended in the orthotopic liver metastasis model, where treatment of MHCC97L cells with FSTL1 nAb attenuated abilities of cells not only led to reduced bioluminescence signal and liver to body weight ratio (**Figure 4E**), but also a marked decrease in number of metastatic nodules detected in the lung (**Figure 4F**).

TLR4 receptor is critical in facilitating FSTL1-mediated hepatocarcinogenesis. Previous studies have found FSTL1 to bind to TLR4, CD14, follistatin (FST) or disco-interaction protein 2 homology A (DIP2A) (35-37). Using HCC data from the TCGA-LIHC dataset, we found FSTL1 expression to be more closely correlated with TLR4 (**Figure 5A**; r=0.46) than as compared to DIP2A (r=0.22), and that CD14 and FST were not associated with FSTL1 (**Supplemental Figure S5**). We then confirmed co-localization and binding of FSTL1 and TLR4 in MHCC97L cells by dual color immunofluorescence and co-immunoprecipitation assays, respectively (**Figure 5B-C**). To functionally characterize the importance of TLR4 in mediating the cancer properties directed by FSTL1, we treated MHCC97L cells with rhFSTL1, in the absence or presence of the specific TLR4 inhibitor, TAK242. Inhibition of TLR4 by TAK242 abrogated rhFSTL1 induced proliferation, migration, invasion, sorafenib resistance and self-renewal capacities (**Figure 5D-H**), suggesting FSTL1 to regulate cancer stemness properties in HCC via the TLR4 axis. Consistently, stable knockdown of TLR4 by lentiviral based shRNA also resulted in similar findings, both *in vitro* and *in vivo* mouse models (**Supplemental Figure S6A-E and S7A-H**). We also investigated on other known receptors of FSTL1 including CD14 and DIP2A, but stable knockdown of CD14 nor DIP2A did not result in any reduced FSTL1-mediated oncogenic effects, suggesting that FSTL1 seems to work primarily through TLR4 in HCC (**Supplemental Figure S8A-J**).

FSTL1 drives hepatocarcinogenesis via a dysregulated AKT/mTOR/4EBP1/c-myc signaling axis. To better understand how CAFs-derived FSTL1 contributes to maintain aggressive cancer properties in HCC, the transcriptome profiles of CAFs, as marked by FAP expression, was analyzed in the HCC tumors of the TCGA LIHC dataset. In the FAP+ CAF subpopulation, genes co-expressed with FSTL1 were subjected for KEGG pathway analysis in DAVID. By this means, we found FSTL1 to be highly associated with PI3K/AKT signaling in HCC patients enriched with CAFs (**Figure 6A**). Consistently, critical molecular players in the AKT/mTOR/c-myc pathway were further confirmed by Western Blot where p-AKT, p-mTOR, p-4EBP1 and c-myc were all found enhanced when MHCC97L HCC cells and HCC patient-derived organoids were treated with either FSTL1 OE CM as compared to EV CM or rhFSTL1 as compared to PBS. Conversely, administration of FSTL1 nAb to the HCC cells and organoids treated with hTERT-HSC CM or FSTL1 OE CM would attenuate the activated signaling (**Figure 6B**). To further validate the significance of AKT driven mTOR/c-myc activation in FSTL1-induced HCC, we analyzed the impact of introducing MK-2206, an inhibitor of AKT, into HCC cells and HCC patient-derived organoids cultured in the presence of rhFSTL1. Successful suppression of AKT/mTOR/4EBP1/c-myc pathway following addition of MK-2206 was confirmed by Western Blot (**Figure 6B**). Functionally, MK-2206 also suppressed the ability of FSTL1-driven HCC cells to proliferate (**Figure 6C and Supplemental Figure S9A**), migrate (**Figure 6D and Supplemental Figure S9B**), invade (**Figure 6E and Supplemental Figure S9B**), resist sorafenib (**Figure 6F and Supplemental Figure S9C**) and self-renew (**Figure 6G and Supplemental Figure S9D**). In line with these findings, inhibition of the more upstream TLR4 by TAK242 also attenuated activation of AKT signaling (**Figure 6I**).

Inhibition of FSTL1 sensitizes HCC tumors to sorafenib, prolonged survival and eradicated the TIC subset in a pre-clinical immunocompetent HCC mouse model. Since we identified FSTL1's ability to confer resistance to sorafenib, we then explored the *in vivo* benefit of targeting FSTL1 in combination with sorafenib in HCC using the NRAS+AKT HTVI immunocompetent HCC mouse model where we found Fstl1 to be overexpressed (**Figure 1B**). FSTL1 nAb and/or sorafenib were administered following HCC formation at 3 weeks and monitored for survival (**Figure 7A**). While sorafenib treatment alone did lead to a decrease in liver to body weight ratio (**Figure 7B**), it did not lead to any survival benefit (**Figure 7C**). But importantly, FSTL1 nAb and sorafenib combination treatment led to a clear decrease not only in liver to body weight ratio, but also enhanced survival as compared to mice treated with

control DMSO+IgG or just sorafenib or FSTL1 nAb alone (**Figure 7B-C**). Subsequent *ex vivo* limiting dilution spheroid formation assays using cells isolated from the liver of this HCC mouse model demonstrated FSTL1 nAb and sorafenib combination to result in the most significant decrease in self-renewal ability of the cells (**Figure 7D**), suggesting FSTL1 nAb to sensitize HCC cells to sorafenib and preferentially eradicated the tumor-initiating subset of the tumor. Immunohistochemical analysis for p-AKT (Ser473) and proliferation marker PCNA expressions in the resected livers of the four treatment groups showed a marked decrease in both p-AKT and PCNA in the FSTL1 nAb and combination treatment groups suggesting FSTL1 nAb did effectively impair AKT signaling and proliferative capacity of the tumor (**Figure 7E**). Dual color immunofluorescence for the epithelial marker pan-cytokeratin and p-AKT (Ser473) confirmed abrogated AKT activation specifically in HCC cells in the two groups treated with FSTL1 nAb (**Figure 7E**). Consistently, we observed a similar activation of p-AKT signaling in tumors driven by FSTL1 overexpressing condition medium; while FSTL1 nAb of these tumors would lead to mitigation of this signaling (**Figure 7F**). Collectively, this data demonstrates the potential of utilizing FSTL1 neutralizing antibody to enhance the efficiency and efficacy of sorafenib.

FSTL1 expression can be maintained by TGF-β1 autocrine signaling in fibroblasts but also potentiated by paracrine signaling from HCC cell lines. To understand how fibroblasts maintain FSTL1 expression, we focused on TGF-β1 as it is reported that FSTL1 expression is governed by TGF-β1 signaling (34). First, we examined the secretory level of TGF-β1 in a panel of immortalized normal liver cell, HCC cells, as well as fibroblasts (**Supplemental Figure S10A**). Of note, the level between HCC cells and fibroblasts are comparable. Furthermore, the secretory level of TGF-β1 and FSTL1 in fibroblasts is highly correlated (**Supplemental Figure S10B**), suggesting that FSTL1 level may be maintained by autocrine signaling of TGF-β1. Using hTERT-HSC and human CAFs as models, we showed that TGF-β1 knockdown in fibroblast resulted in a significant reduction of FSTL1 expression at the mRNA and protein level (**Supplemental Figure S10C-H**). Consistently, TGF-β1 neutralizing antibody diminished the production of secretory FSTL1 (**Supplemental Figure S10I-J**). Computational analysis by JASPAR identified three binding sites of the major downstream effector of TGF-β, SMAD2/3/4, on the promoter of FSTL1 (**Supplemental Figure S10K**). Further analysis by LASAGNA showed SMAD4 to be a top hit as a transcription factor regulating FSTL1 expression. Further

experiments whereby SMAD4 was knocked down by siRNA approach found FSTL1 expression to be decreased (**Supplemental Figure S10L**), which further confirms that fibroblast-derived TGF-β1/SMAD4 signaling plays a role in the control of FSTL1 through an autocrine manner.

In lights of the secretory TGF-β1 level in HCC cells, we also reasoned that HCC cells can mediate crosstalk with fibroblast via TGF-β1 paracrine signaling. To this end, we cultured fibroblasts with conditioned media collected from HCC cells with TGF-β1 suppressed (**Supplemental Figure S11A**). Compared to the siNTC control, conditioned media of TGF-β1 knockdown HCC cells showed diminished ability to promote FSTL1 production in the fibroblasts (**Supplemental Figure S11B-C**). In accordance, HCC cells conditioned media treated with TGF-β1 neutralizing antibody demonstrated reduced ability to stimulate FSTL1 (**Supplemental Figure S11D-E**). Thus, our results depicted HCC to fibroblast crosstalk via TGF-β1 signaling can enhance production of FSTL1 from fibroblasts, in turn, potentiates malignant properties of HCC cells.

DISCUSSION

The limited options and modest efficacy of drugs for advanced HCC urge for the development of novel treatment. Given most HCC develops in a fibrosis or cirrhosis liver, how a highly inflammatory TME contributes hepatocarcinogenesis warrants further investigation. Here, we demonstrated Fstl1 expression is upregulated in cirrhosis, regenerative and disease state, as evident in liver regeneration model, DEN+CCL_4 fibrotic HCC model, and hydrodynamic tail vein injection HCC model. RNA-seq of DEN+CCL_4 fibrotic model depicted several CAF-secreted genes to be elevated in tumor compared to vehicle control. Of interest, among the other reported known activated fibroblast-derived factors like Ctgf, Igf2, Tnf, Ccl5, Pdgfc (38-39), we find levels of Fstl1 to be expressed at high levels in HCC versus vehicle control. A high correlation between Acta2 and Fstl1 gene expression was observed in all mouse models. Additionally, FSTL1 secretory level is substantially greater in HCC patient-derived fibroblast lines compared to HCC cell lines while immunofluorescence depicted colocalization ACTA2 and FSTL1. Together, we reasoned that FSTL1 is preferentially secreted from the fibroblasts. Using tamoxifen-inducible FSTL1 reporter *Fstl1-CreERT2;Rosa26-mT-mG* (33), we showed FSTL1 lineage cells to give rise to αSMA+ fibroblasts in CCL_4 induced liver fibrosis, indicating FSTL1 as an important growth factor involved in promoting growth upon injury in the liver. Another study found FSTL1 to be elevated in HCC tissue compared to the adjacent non-tumor liver tissue and high FSTL1 was associated with poor prognosis (40). As such, we demonstrated that FSTL1 protein level was higher in CAF CM compared to NF CM, alluding to the possibility of cancer cells being modulated by FSTL1 expression to accelerate their growth (41). FSTL1 may be used as a potential prognostic marker as more advanced TNM staging in HCC patients was associated with high FSTL1 in FAP+ fibroblasts. It is worthy to note that FSTL1 has been shown in one study to be elevated in HCC cancer cells (40). This is contrary to our study where we found FSTL1 to be predominantly expressed from activated fibroblasts and that FSTL1 is only secreted at very low levels, if at all, in HCC cancer cells. We suspect that authors in the study Yang et al. did not explore into other cell types other than HCC cells; so while it is possible that HCC cells may secrete some expression of FSTL1, majority of the source is not from there.

The crosstalk between CAF and TICs is pivotal for cancer progression (42). In this study, we revealed FSTL1, which is elevated during fibrosis, promotes stemness of liver cancer cells. FSTL1 OE CM and

rhFSTL1 both promote proliferation, stem cell frequency, migration and invasion, and therapy resistance in MHCC97L HCC cell line and HCC patient-derived organoid. Complementary *in vivo* studies further confirmed the tumorigenic and metastatic functions of FSTL1 in HCC. The malignant properties driven by FSTL1 in HCC are consistent with other studies done on esophageal, liver, colon and breast cancers (20-22, 40, 43). However, FSTL1 was reported to function as tumor suppressor in renal cell carcinoma and lung cancer (44-45), illustrating FSTL1 facilitates as an oncogene or tumor suppressor gene in a tissue-dependent manner. Here, we demonstrated FSTL1 mediates its oncogenic influence via TLR4, a binding receptor which has been shown to be involved in HCC progression (46-47).

A systematic analysis of the transcriptomes of HCC patients enriched with CAF found the PI3K/AKT signaling pathway to be highly associated with FSTL1. AKT/mTORC1 regulates protein synthesis predominantly through two independent effectors, 4EBP and S6K1. Upon activation, mTORC1 phosphorylates 4EBP, triggering the release of eukaryotic translation initiation factor 4E (eIF4E), which is essential for translation initiation. Studies have also demonstrated that mTORC1 signaling is essential for c-myc-driven HCC progression (48); with 4EBP1/eIF4E regulating c-myc translational levels (49). There is also ample literature to show the crucial role of c-myc in hepatocarcinogenesis (50-52). In regard to the upstream regulator of mTOR, AKT is known to control mTOR signaling (53), while FSLT1 has also been shown to function through AKT (40, 54). Accordingly, we explored if FSTL1 regulates mTOR/c-myc pathway through AKT activation in HCC. We showed that inhibiting AKT using MK-2206 resulted in the ablation of FSTL1-mediated malignancy and reduced activation of mTOR signaling as analyzed using western blot, hence providing robust evidence that FSTL1 functions via the AKT/mTORC1/4EBP/c-myc axis in HCC cells. Our study postulates an interesting link between elevated FSTL1 in fibrosis state and FSTL1-driven c-myc, alluding to a possible link of how fibrosis may fuel hepatocyte transformation by elevating AKT/mTOR/c-myc signaling.

Ever since the discovery of TICs, numerous strategies have been explored to target TICs (55). However, TME, which functions as the TIC niche can restore the eradicated TIC population. Moreover, TME-derived autocrine and paracrine factors are essential for the maintenance of TIC phenotype. Therefore, targeting oncogenic growth factors in the TME presents an intriguing option to circumvent

TIC phenotype. We explore the potential of attenuating CAF-derived FSTL1-driven malignancy by using FSTL1 neutralizing antibody (19). Similarly observed in our previous study which demonstrated targeting FSTL1 with neutralizing antibody in esophageal cancer can circumvent the oncogenic effect (21), we demonstrated treating FSTL1 OE CM with neutralizing antibody can hinder the oncogenic properties and restore the HCC cells to the level comparable to EV CM. Further *in vivo* functional assay investigating growth, stemness and metastasis recapitulated the *in vitro* results. To evaluate the translational value of inhibiting FSTL1, we tested the efficacy of FSTL1 neutralizing antibody in combination with sorafenib in an immunocompetent preclinical model. Strikingly, our results indicated administration of sorafenib with FSTL1 nAb markedly extended the survival of the mice, possibly by suppressing the self-renewal and proliferative ability conferred by FSTL1. In sum, our findings showed targeting FSTL1 presents clinical relevance in treating HCC. In conjunction with other studies like for instance targeting CAF-secreted Netrin-1 in lung and colon cancers (27), we provide evidence that targeting CAF-secreted factors may hold therapeutic value.

In conclusion, FSTL1, a growth factor secreted by activated fibroblasts, augments malignancy and holds potential clinical value as a prognostic marker and therapeutic target, particularly in patients with high FAP and FSTL1 expression. Our findings illuminate FSTL1 confers HCC progression by enhancing TIC features of the HCC via TLR4-mediated AKT/mTORC/4EBP/c-myc signaling axis.

ACKNOWLEDGEMENTS

This project is supported in part by grants from the Research Grants Council of Hong Kong – Theme Based Research Scheme (T12-704/16-R) and Collaborative Research Fund (C7026-18G), Health and Medical Research Fund from Food and Health Bureau of the Hong Kong Government (06172546) as well as the "Laboratory for Synthetic Chemistry and Chemical Biology" under the Health@InnoHK Program launched by Innovation and Technology Commission, The Government of Hong Kong Special Administration Region of the People's Republic of China. We thank the Centre for PanorOmic Sciences (The University of Hong Kong) for providing and maintaining the equipment and technical support needed for flow cytometry, animal imaging and confocal microscopy studies. We thank the Centre for Comparative Medicine Research (The University of Hong Kong) for supporting our animal work studies.

AUTHOR CONTRIBUTIONS

JJL, NTWL, MT and SM conceived the project and designed the studies. JJL and NTWL performed the research, analyzed and interpreted the data, with the help of LZ, TLW and MT. VWSM performed multiple immunofluorescence on formalin-fixed paraffin-embedded tissues. CML and KM obtained patient consent and provided clinical samples for HCC organoid culture. XYG provided reagents. XL and WN performed the research, analyzed and interpreted the data of Fstl1 lineage tracing experiments. WN provided FSTL1 neutralizing antibodies. TKW provided reagents and critical scientific input. JJL, MT and SM wrote the paper. MT and SM supervised the project and provided funding for the study.

REFERENCES

1. Bray F, Ferlay J, Soerjomataram I, Siegel RL, Torre LA, Jemal A. Global cancer statistics 2018: GLOBOCAN estimates of incidence and mortality worldwide for 36 cancers in 185 countries. CA Cancer J Clin 2018; 68:394-424.
2. El-Serag HB. Hepatocellular carcinoma. N Engl J Med 2011; 365:1118-27.
3. Fattovich G, Stroffolini T, Zagni I, Donato F. Hepatocellular carcinoma in cirrhosis: incidence and risk factors. Gastroenterology 2004; 127:35-50.
4. Affo S, Yu LX, Schwabe RF. The role of cancer-associated fibroblasts and fibrosis in liver cancer. Annu Rev Pathol 2017; 12:153-86.
5. Capece D, et al. The inflammatory microenvironment in hepatocellular carcinoma: a pivotal role for tumor-associated macrophages. Biomed Res Int 2013; 187204.
6. Bouattour M, Mehta N, He AR, Cohen EI, Nault JC. Systemic treatment for advanced hepatocellular carcinoma. Liver Cancer 2019; 8:341-58.
7. Llovet JM, et al. Sorafenib in advanced hepatocellular carcinoma. N Engl J Med 2008; 359:378-90.
8. Reya T, Morrison SJ, Clarke MF, Weissman IL. Stem cells, cancer, and cancer stem cells. Nature 2001; 414:105-11.
9. Prager BC, Xie Q, Bao S, Rich JN. Cancer stem cells: the architects of the tumor ecosystem. Cell Stem Cell 2019; 24:41-53.
10. Vermeulen L, et al. Wnt activity defines colon cancer stem cells and is regulated by the microenvironment. Nat Cell Biol 2010; 12:468-76.
11. Tsuyada A, et al. CCL2 mediates cross-talk between cancer cells and stromal fibroblasts that regulates breast cancer stem cells. Cancer Res 2012; 72:2768-79.
12. Lau EY, et al. Cancer-associated fibroblasts regulate tumor-initiating cell plasticity in hepatocellular carcinoma through c-Met/FRA1/HEY1 signaling. Cel Rep 2016; 15:1175-89.
13. Su S, et al. CD10+ GPR77+ cancer-associated fibroblasts promote cancer formation and chemoresistance by sustaining cancer stemness. Cell 2018; 172:841-56.
14. Ren Y, et al. Paracrine and epigenetic control of CAF-induced metastasis: the role of HOTAIR stimulated by TGF-β1 secretion. Mol Cancer 2018; 17:5.

15. Paauwe M, et al. Endoglin expression on cancer-associated fibroblasts regulates invasion and stimulates colorectal cancer mestastasis. Clin Cancer Res 2018; 24: 6331-44.
16. Wen S, et al. Cancer-associated fibroblast (CAF)-derived IL32 promotes breast cancer cell invasion and metastasis via integrin β3-p38 MAPK signaling. Cancer Lett 2019; 442:320-32.
17. Miyamae T, et al. Follistain-like protein-1 is a novel proinflammatory molecule. J Immunol 2006; 177:4758-62.
18. Miaruyama S, et al. Follistatin-like 1 promotes cardiac fibroblast activation and protects the heart from rupture. EMBO Mol Med 2016; 8:949-66.
19. Dong Y, et al. Blocking follistatin-like 1 attenuates bleomycin-induced pulmonary fibrosis in mice. J Exp Med 2015; 212:1118-27
20. Cheng S, Huang Y, Lou C, He Y, Zhang Y, Zhang Q. FSTL1 enhances chemoresistance and maintains stemness in breast cancer cells via integrin beta3/Wnt signaling under miR-137 regulation. Cancer Biol Ther 2019; 20:328-37.
21. Lau MC, et al. FSTL1 promotes metastasis and chemoresistance in esopahgeal squamous cell carcinoma through NFkappaB-BMP signaling cross-talk. Cancer Res 2017; 77:5886-99.
22. Gu C, et al. FSTL1 interacts with VIM and promotes colorectal cancer metastasis via activating the focal adhesion signaling pathway. Cell Death Dis 2018; 9:654.
23. Schnabl B, Choi YH, Olsen JC, Hagedorn CH, Brenner DA. Immortal activated human hepatic stellate cells generated by ectopic telomerase expression. Lab Invest 2002; 82:323-33.
24. Chan LH, et al. PRMT6 regulates RAS/RAF binding and MEK/ERK-mediated cancer stemness activities in hepatocellular carcinoma through CRAF methylation. Cell Rep 2018; 25:690-701.
25. Tong M, et al. Efficacy of annexin A3 blockade in sensitizing hepatocellular carcinoma to sorafenib and regorafenib. J Hepatol 2018; 69:826-39.
26. Huch M, et al. Long-term culture of genome-stable bipotent stem cells from adult human liver Cell 2015; 160:299-312.
27. Sung PJ, et al. Cancer-associated fibroblasts produce netrin-1 to control cancer cell plasticity. Cancer Res 2019; 79:3651-61.
28. Zou B, et al. A novel 12-marker panel of cancer-associated fibroblasts involved in progression of hepatocellular carcinoma. Cancer Manag Res 2018; 10: 5303-11.

29. Ma S, et al. Identification and characterization of tumorigenic liver cancer stem/progenitor cells. Gastroenterology 2007; 132:2542-56.
30. Uehara T, Pogribny IP, Rusyn I. The DEN and CCl4-induced mouse model of fibrosis and inflammation-associated hepatocellular carcinoma. Curr Protoc Pharmacol 2014; 66:1-10.
31. Chen X, Calvisi DF. Hydrodynamic transfection for generation of novel mouse models for liver cancer research. Am J Pathol 2014; 184:912-23.
32. Ho C, et al. AKT (v-akt murine thymoma viral oncogene homolog 1) and N-Ras (neuroblastoma ras viral oncogene homolog) coactivation in the mouse liver promotes rapid carcinogenesis by way of mTOR (mammalian target of rapamycin complex 1), FOXM1 (forkhead box M1)/SKP2, and c-Myc pathways. Hepatology 2012; 55:833-45.
33. Liu X, Liu Y, Yang Z, Ning W. Cell type specific expression of follistain-like 1 (Fstl1) in mouse embryonic lung development. J Mol Histol 2018; 49:399-409.
34. Zheng X, Qi C, Zhang S, Fang Y, Ning W. TGF-β1 induces Fstl1 via the Smad3-c-Jun pathway in lung fibroblasts. Am J Physiol Lung Cell Mol Physiol 2017; 313:L240-51.
35. Geng Y, et al. Follistatin-like 1 (Fstl1) is a bone morphogenetic protein (BMP) 4 signaling antagonist in controlling mouse lung development. Proc Natl Acad Sci USA 2011; 108: 7058-63.
36. Murakami K, et al. Follistatin-related protein/follistatin-like 1 evokes an innate immune response via CD14 and toll-like receptor 4. FEBS Lett 2012; 586:319-24.
37. Ouchi N, et al. DIP2A functions as a FSTL1 receptor. J Biol Chem 2010; 285:7127-34.
38. Kalluri R. The biology and function of fibroblasts in cancer. Nat Rev Cancer 2016; 16:582-98.
39. Kobayashi H, Enomoto A, Woods SL, Burt AD, Takahashi M, Worthley DL. Cancer-associated fibroblasts in gastrointestinal cancer. Nat Rev Gastroenterol Hepatol 2019; 16:282-95.
40. Yang W, Wu Y, Wang C, Liu Z, Xu M, Zheng X. FSTL1 contributes to tumor progression via attenuating apoptosis in a AKT/GSK-3β-dependent manner in hepatocellular carcinoma. Cancer Biomark 2017; 20:75-85.
41. Kalluri R, Zeisberg M. Fibroblasts in cancer. Nat Rev Cancer 2006; 6:392-401.
42. Huang TX, Guan XY, Fu L. Therapeutic targeting of the crosstalk between cancer-associated fibroblasts and cancer stem cells. Am J Cancer Res 2019; 9:1889-904.
43. Bevivino G, et al. Follistatin-like protein 1 sustains colon cancer cell growth and survival. Oncotarget 2018; 9:31278-90.

44. Liu Y, et al. Follistain-like protein 1 plays a tumor suppressor role in clear-cell renal cell carcinoma. Chin J Cancer 2018; 37:2.
45. Ni X, Cao X, Wu Y, Wu J. FSTL1 suppresses tumor cell proliferation, invasion and survival in non-small cell lung cancer. Oncol Rep 2018; 39:13-20.
46. Dapito DH, et al. Promotion of Hepatocellular Carcinoma by the Intestinal Microbiota and TLR4. Cancer Cell 2012; 21:504-16
47. Lin A, et al. TLR4 signaling promotes a COX-2/PGE2/STAT3 positive feedback loop in hepatocellular carcinoma (HCC) cells. Oncoimmunology; 5:e1074376
48. Liu P, et al. A functional mTORC1 signaling is indispensable for c-myc driven hepatocarcinogenesis. Hepatology 2017; 66:167-81.
49. Hu G, Lou Z, Gupta M. The long non-coding RNA GAS5 cooperates with the eukaryotic translation initiation factor 4E to regulate c-Myc translation. PLoS One 2014; 9:e107016.
50. Akita H, et al. MYC activates stem cell-like cell potential in hepatocarcinoma by a p53-dependent mechanism. Cancer Res 2014; 74:5903-13.
51. Qu A, et al. Role of myc in hepatocellular proliferation and hepatocarcinogenesis. J Hepatol 2014; 60:331-8.
52. Chow EK, Fan LL, Chen X, Bishop JM. Oncogene-specific formation of chemoresistant murine hepatic cancer stem cells. Hepatology 2012; 56:1331-41.
53. Porta C, Paglino C, Mosca A. Targeting PI3K/Akt/mTOR signaling in cancer. Front Oncol 2014; 4:64.
54. Liang X, et al. Follistain-like 1 attenuates apoptosis via disco-interacting protein 2 homolog A/Akt pathway after middle cerebral artery occlusion in rats. Stroke 2014; 45:3048-54.
55. Shibata M, Hoque MO. Targeting cancer stem cells: a strategy for effective eradication of cancer. Cancers 2019; 11.

FIGURE LEGENDS

***Fstl1*/FSTL1 expression is closely correlated with activated fibroblasts and elevated in regenerative, fibrotic and disease states in various mouse models of the liver and in human HCC. (A)** Schematic representation of the 70% partial hepatectomy liver regeneration model in C57BL/6 mice used in this study. qPCR analysis of *Fstl1* expression at 0, 1.5, 3 and 7 days post-hepatectomy. Pearson correlation analysis of *Fstl1* and *Acta2* expression in mice samples. **(B)** Schematic representation of the hydrodynamic tail vein injection (HTVI) HCC model in C57BL/6 mice used in this study. NRAS+AKT used as oncogenic plasmid combination to induce HCC with sleeping beauty (SB) transposase. qPCR analysis of *Fstl1* expression at 1 to 5 weeks post plasmids injection. Pearson correlation analysis of *Fstl1* and *Acta2* expression in mice samples. **(C)** Schematic representation of the DEN+CCL_4 fibrosis-induced HCC model in C57BL/6 mice used in this study. qPCR analysis of *Fstl1* expression at 8 to 24 weeks. 8 weeks represent normal liver, 16 to 20 weeks represent fibrotic liver and 22 to 24 weeks represent HCC. Pearson correlation analysis of *Fstl1* and *Acta2* expression in mice samples. **(D)** Schematic representation of Fstl1 reporter (*Fstl1-CreERT2;Rosa26-mT-mG*) mouse generation. Fstl1-expressing cells were labeled green upon tamoxifen treatment. Model 1 – induce fibrosis by CCL_4 treatment followed by tamoxifen administration for Fstl1 tracing. Model 2 – Tamoxifen administration for Fstl1 tracing prior to induction of fibrosis by CCL_4 treatment. Representative immunofluorescence images for Fstl1 (green) and αSMA (red) expression in the liver of the two models. DAPI (blue) to mark nucleus. **(E)** Measurement of secretory FSTL1 levels in a panel of immortalized normal liver (MIHA), HCC cell lines (MHCC97L, MHCC97H, SNU878, HepG2, PLC8024, Huh7 and Hep3B), normal fibroblast, hTERT-HSC and 3 pairs of patient-derived non-tumor liver (NF) and adjacent HCC derived fibroblasts (CAF) by ELISA. Secretory FSTL1 of conditioned medium (CM) generated from CHO-K1 transfected with empty vector (EV) control and FSTL1 overexpression (OE) plasmids also recorded. **(F)** Pearson correlation analysis of CAF score versus FSTL1 expression. **(G)** Representative immunofluorescence images for FSTL1 (green) and αSMA (red) in human non-tumor liver and adjacent HCC tissue sample. DAPI (blue) to mark nucleus. **(H)** Representative immunofluorescence images for FSTL1 (green) and αSMA (red) in two additional HCC tissue samples. DAPI (blue) to mark nucleus. **(I)** Pearson correlation analysis of FSTL1 and ACTA2 expression in non-tumor liver/HCC samples in our in-house samples (top). Pearson correlation analysis of FSTL1 and FAP expression in non-tumor liver/HCC samples in the TCGA-LIHC cohort (bottom). **(J)** TCGA LIHC analysis

of correlation between TNM stage and $FAP^{high}/FSTL1^{low}$ (*n*=95) or $FAP^{high}/FSTL1^{high}$ (*n*=89) HCC patients. DEN for diethylnitrosamine. CCL_4 for carbon tetrachloride. Smooth muscle α actin (Acta2) representative of myofibroblasts. Fibroblast activation protein (FAP) representative of activated fibroblasts. TCGA LIHC for The Cancer Genome Atlas – Liver Hepatocellular Carcinoma. *, **, *** and **** for $p<0.05$, $p<0.01$, $p<0.001$ and $p<0.0001$, respectively.

Figure 2. FSTL1 promotes malignant properties in HCC cells *in vitro* and *in vivo*. (A-C, left) Representative images and quantitation of number of cells that formed foci (A), migrated (B) or invaded (C) in MHCC97L cells treated with empty vector conditioned medium (EV CM) control or FSTL1 overexpressing conditioned medium (FSTL1 OE CM). **(A-C, right)** Representative images and quantitation of number of cells that formed foci (A), migrated (B) or invaded (C) in MHCC97L cells treated with PBS control or recombinant FSTL1 (rhFSTL1). Scale bar = 5mm for panel A. Scale bar = 100μm for panels B and C. **(D)** Annexin V PI analysis for number of apoptotic/necrotic cells when MHCC97L cells treated with EV CM vs. FSTL1 OE CM or PBS vs. rhFSTL1 were challenged with DMSO control or sorafenib. **(E)** *In vitro* limiting dilution analysis for frequency of tumor-initiating cells in MHCC97L cells treated with EV CM vs. FSTL1 OE CM or PBS vs. rhFSTL1. **(F, left)** Measurement of tumor volume in nude mice subcutaneously injected with MHCC97L cells treated with empty vector conditioned medium (EV CM) control or FSTL1 overexpressing conditioned medium (FSTL1 OE CM). **(F, right)** Image of resected xenografts. Scale bar = 1cm. *n*=8 mice per group. **(G)** Kaplan-Meier curve showing percentage of tumor-free survival of NOD-SCID mice injected with MHCC97L cells treated with EV CM vs. FSTL1 OE CM. **(H)** *Ex vivo* limiting dilution analysis for frequency of tumor-initiating cells using tumors harvested from the 20,000 cell group of subcutaneous xenografts. *n*=10 mice per group. (**I, top**) Bioluminescence imaging and image of resected xenografts of nude mice injected intrahepatically with luciferase-labeled MHCC97L cells treated with EV CM vs. FSTL1 OE CM. *n*=6 mice per group. Scale bar = 1cm. **(I, bottom)** Luciferase signal quantitation of the bioluminescence images shown on top and liver to body weight ratio of the intrahepatic metastasis mouse model. **(J)** Bar chart summary of number of metastatic foci observed in the lung tissues. Representative H&E staining of lung tissues harvested from the intrahepatic metastasis model. Yellow box depicts representative metastatic foci where nucleus of cells are enlarged and cells look more irregular. PI for propidium

iodide; H&E for hematoxylin and eosin. *, **, *** and **** for $p<0.05$, $p<0.01$, $p<0.001$ and $p<0.0001$, respectively.

Figure 3. Blockade of FSTL1 by a specific monoclonal neutralizing antibody mitigates HCC malignancy *in vitro*. (A-C) Representative images and quantitation of number of cells that formed foci (A), migrated (B) or invaded (C) in MHCC97L cells treated with hTERT-HSC with IgG or FSTL1 neutralizing antibody (nAb); empty vector conditioned medium (EV CM) + IgG control or FSTL1 overexpressing conditioned medium (FSTL1 OE CM) + IgG control or FSTL1 OE CM + FSTL1 nAb. Scale bar = 5mm for panel A. Scale bar = 100μm for panels B and C. **(D)** Annexin V PI analysis for number of apoptotic/necrotic cells when MHCC97L cells treated with hTERT-HSC with IgG or FSTL1 nAb; EV CM + IgG control vs. FSTL1 OE CM + IgG control vs. FSTL1 OE CM + FSTL1 nAb were challenged with DMSO control or sorafenib. **(E)** *In vitro* limiting dilution analysis for frequency of tumor-initiating cells in MHCC97L cells treated with hTERT-HSC with IgG or FSTL1 nAb; EV CM + IgG control vs. FSTL1 OE CM + IgG control vs. FSTL1 OE CM + FSTL1 nAb. PI for propidium iodide. *, ** and *** for $p<0.05$, $p<0.01$ and $p<0.001$, respectively.

Figure 4. Neutralization of FSTL1 attenuates HCC malignancy *in vivo*. (A, left) Measurement of tumor volume and tumor weight in nude mice injected with MHCC97L cells treated with empty vector conditioned medium (EV CM) + IgG controls or FSTL1 overexpressing conditioned medium (FSTL1 OE CM) + IgG control or FSTL1 OE CM + FSTL1 neutralizing antibody (nAb). **(A, right)** Image of resected xenografts. Scale bar = 1cm. n=8 mice per group. **(B)** Kaplan-Meier curves showing percentage of tumor-free survival of NOD-SCID mice injected with MHCC97L cells treated with EV CM + IgG controls vs. FSTL1 OE CM + IgG control vs. FSTL1 OE CM + FSTL1 nAb in primary and secondary implantations. **(C)** Image of resected xenografts from secondary implantation. Scale bar = 1cm. n=7 mice per group. **(D)** *Ex vivo* limiting dilution analysis for frequency of tumor-initiating cells using tumors harvested from the 20,000 cell group of subcutaneous xenografts. **(E, top)** Bioluminescence imaging and image of resected xenografts of nude mice injected intrahepatically with luciferase-labeled MHCC97L cells treated with EV CM + IgG controls vs. FSTL1 OE CM + IgG control vs. FSTL1 OE CM + FSTL1 nAb. n=6 mice per group. Scale bar = 1cm. **(E, bottom)** Luciferase signal quantitation of the bioluminescence images shown on top and liver to body weight ratio of the intrahepatic metastasis mouse model. **(F)**

Bar chart summary of number of metastatic foci observed in the lung tissues. Representative H&E staining of lung tissues harvested from the intrahepatic metastasis model. Yellow box depicts representative metastatic foci where nucleus of cells are enlarged and cells look more irregular. H&E for hematoxylin and eosin. *, **, *** and **** for $p<0.05$, $p<0.01$, $p<0.001$ and $p<0.0001$, respectively.

Figure 5. TLR4 receptor is critical in facilitating FSTL1-mediated hepatocarcinogenesis. (A) Pearson correlation analysis of FSTL1 and TRL4 mRNA expressions in HCC samples in the TCGA-LIHC cohort. **(B)** Representative immunofluorescence for co-localization of FSTL1 and TLR4 in MHCC97L cells. DAPI (blue) to mark nucleus. Histogram representation of line scan analysis for quantification of FSTL1 and TLR4 relative to DAPI. **(C)** Co-immunoprecipitation analysis for validation of TLR4 as an interacting protein partner of FSTL1 in MHCC97L cells. **(D-F)** Representative images and quantitation of number of cells that formed foci (D), migrated (E) or invaded (F) in MHCC97L cells treated with DMSO control, recombinant FSTL1 (rhFSTL1) or rhFSTL1 plus TLR4 inhibitor TAK242. Scale bar = 5mm for panel D. Scale bar = 100μm for panels E and F. **(G)** Annexin V PI analysis for number of apoptotic/necrotic cells when MHCC97L cells treated with DMSO control, recombinant FSTL1 (rhFSTL1) or rhFSTL1 plus TLR4 inhibitor TAK242 were challenged with DMSO control or sorafenib. **(H)** *In vitro* limiting dilution analysis for frequency of tumor-initiating cells in MHCC97L cells treated DMSO control, recombinant FSTL1 (rhFSTL1) or rhFSTL1 plus TLR4 inhibitor TAK242. **(I)** Western Blot analysis for expression of phosphorylated and total AKT in MHCC97L cells in the presence of rhFSTL1 with or without TAK242. PI for propidium iodide. *, ** and *** for $p<0.05$, $p<0.01$ and $p<0.001$, respectively.

Figure 6. FSTL1 drives hepatocarcinogenesis via a dysregulated AKT/mTOR/4EBP1/c-myc signaling axis. (A) KEGG pathway analysis by DAVID found FSTL1 to be highly associated with PI3K-AKT signaling in HCC patient samples enriched with CAFs. **(B)** Western Blot analysis for expression of phosphorylated and total AKT, phosphorylated and total mTOR, phosphorylated and total 4EBP1 and c-myc in MHCC97L cells and HCC patient-derived organoids treated with EV CM vs. FSTL1 OE CM or PBS vs. rhFSTL1 or hTERT-HSC CM + IgG vs. hTERT-HSC CM + FSTL1 nAb or EV CM + IgG vs. FSTL1 OE CM + IgG vs. FSTL1 OE CM + FSLT1 nAb or DMSO vs. rhFSTL1 vs. rhFSTL1 + MK-2206. **(C-E)** Representative images and quantitation of number of cells that formed foci (C), migrated (D) or

invaded (E) in MHCC97L cells treated with DMSO control vs. rhFSTL1 vs. rhFSTL1 + MK-2206. Scale bar = 5mm for panel D. Scale bar = 100μm for panels E and F. **(F)** Annexin V PI analysis for number of apoptotic/necrotic cells when MHCC97L cells treated with DMSO control vs. rhFSTL1 vs. rhFSTL1 + MK-2206 were challenged with DMSO control or sorafenib. **(G)** *In vitro* limiting dilution analysis for frequency of tumor-initiating cells in MHCC97L cells treated with DMSO control vs. rhFSTL1 vs. rhFSTL1 + MK-2206. NES for normalized enrichment score. FDR for false discovery rate. EV CM for empty vector conditioned medium control. FSTL1 OE CM for FSTL1 overexpressing conditioned medium. rhFSTL1 for recombinant FSTL1. nAb for neutralizing antibody. MK-2206 is an AKT inhibitor. PI for propidium iodide. *, ** and *** for $p<0.05$, $p<0.01$ and $p<0.001$, respectively.

Figure 7. Inhibition of Fstl1 sensitizes HCC tumors to sorafenib, prolonged survival and eradicated the TIC subset in a pre-clinical immunocompetent HCC mouse model. (A) Schematic diagram of the treatment regimen with DMSO+IgG (group 1), sorafenib+IgG (group 2), DMSO+FSTL1 neutralizing antibody (nAb) (group 3) and sorafenib+FSTL1 nAb (group 4) in a NRAS+AKT HTVI HCC mouse model. n=11-12 mice per group. **(B)** Graphs showing liver to body weight ratio generated from the model. **(C)** Kaplan-Meier survival curve showing percentage of tumor-free survival of each annotated group. **(D)** *Ex vivo* limiting dilution analysis for frequency of tumor-initiating cells using tumors harvested from pooled groups of subcutaneous xenografts. **(E)** H&E and immunohistochemical staining for p-AKT (Ser473) and PCNA in HCC tumors harvested from the 4 treatment groups. Representative immunofluorescence images for epithelial marker pan-cytokeratin (green) and p-AKT (Ser473) (red) in HCC tumors harvested from the 4 treatment groups. DAPI (blue) to mark nucleus. **(F)** Immunohistochemical staining for p-AKT (Ser473) in HCC tumors of EV CM, FSTL1 OE CM, EV CM+IgG, FSTL1 OE CM+IgG and FSTL1 OE CM+nAb treatment groups in *in vivo* models. SB for sleeping beauty transposase. EV for empty vector, OE for overexpression, CM for conditioned medium. *, ** and **** for $p<0.05$, $p<0.01$ and $p<0.0001$, respectively.

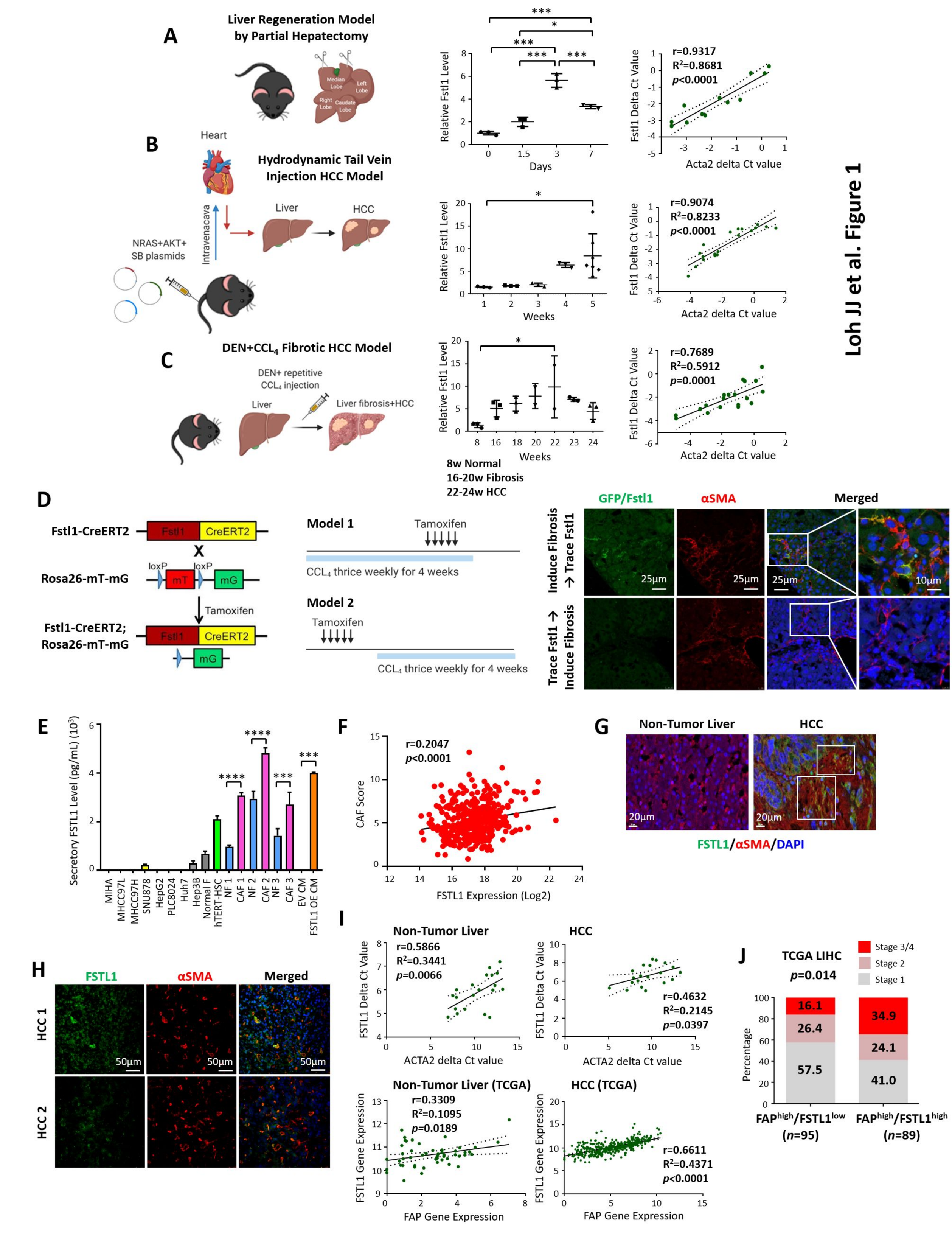

Loh JJ et al. Figure 1

Loh JJ et al. Figure 2

MHCC97L

A
Proliferation
EV CM
FSTL1 OE CM
No. of Foci Formed
EV CM
OE CM
PBS
rhFSTL1
No. of Foci Formed
PBS
rhFSTL1

B
Migration
No. of Migrating Cells
EV CM
OE CM
No. of Migrating Cells
PBS
rhFSTL1

C
Invasion
No. of Invading Cells
EV CM
OE CM
No. of Invading Cells
PBS
rhFSTL1

D
EV CM
FSTL1 OE CM
PBS
rhFSTL1
DMSO
5.8%
6.6%
8.1%
8.2%
Sorafenib
56.7%
30.4%
55.1%
31.4%
PI
Annexin V
Apoptosis (%)
EV CM
OE CM
Apoptosis (%)
PBS
rhFSTL1

E
Log Fraction Non-responding
EV CM
1:30
OE CM
1:17
Number of cells
PBS
1:6
rhFSTL1
1:4
Number of cells

F
Tumor Volume (mm³)
OE CM
EV CM
Days Post-Injection
OE CM
EV CM

G
Tumor Free Survival (%)
EV CM
OE CM
Days Post-Injection

H
Log Fraction Non-responding
EV CM
1:93
OE CM
1:25
Number of Cells

I
EV CM
OE CM
Luminescence x10⁹
Radiance (p/sec/cm²/sr)
Color Scale
Min = 5.28e7
Max = 9.40e8
OE CM
EV CM

J
Arbitrary Luciferase (x10⁸)
EV CM
OE CM
Liver/Body Weight Ratio
EV CM
OE CM
No. of Metastatic Nodules
EV CM
OE CM

Lung
EV CM
100μm
50μm
OE CM

MHCC97L

A

HSC CM + IgG | HSC CM + nAb

Proliferation

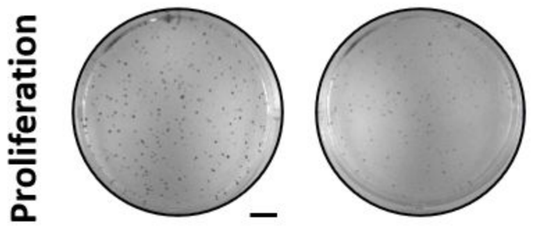

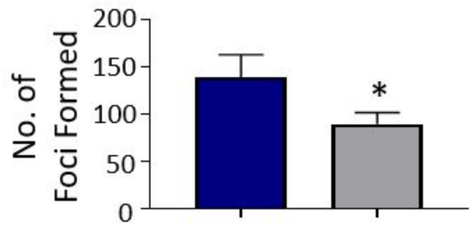

EV CM + IgG | OE CM + IgG | OE CM + nAb

Proliferation

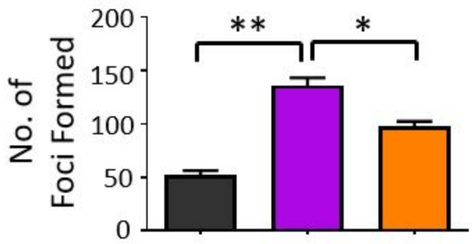

B

Migration

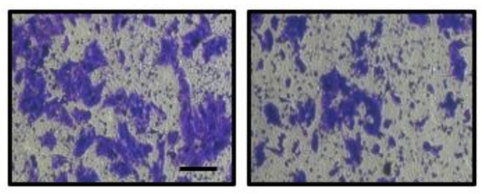

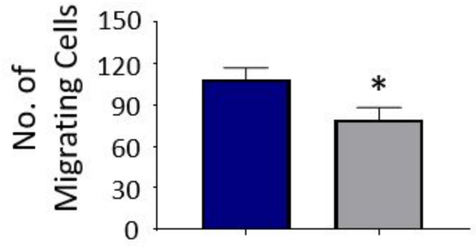

Migration

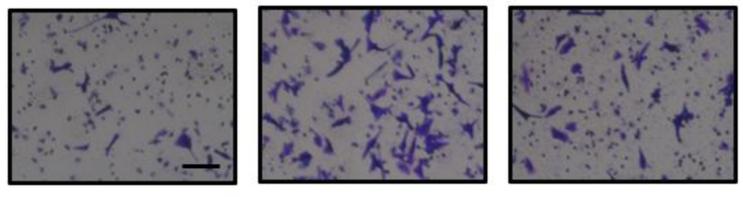

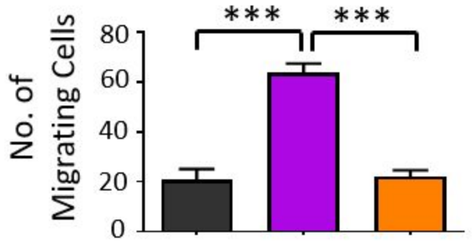

C

Invasion

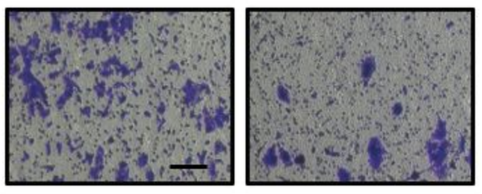

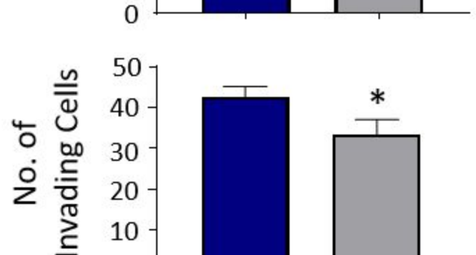

Invasion

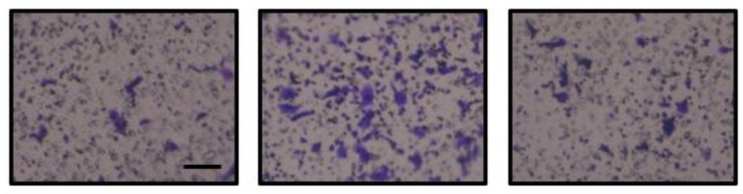

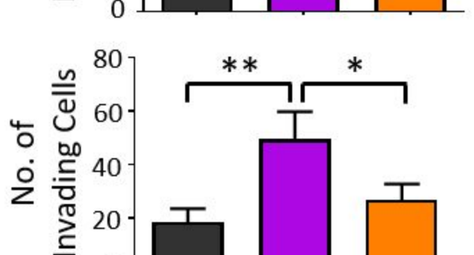

D

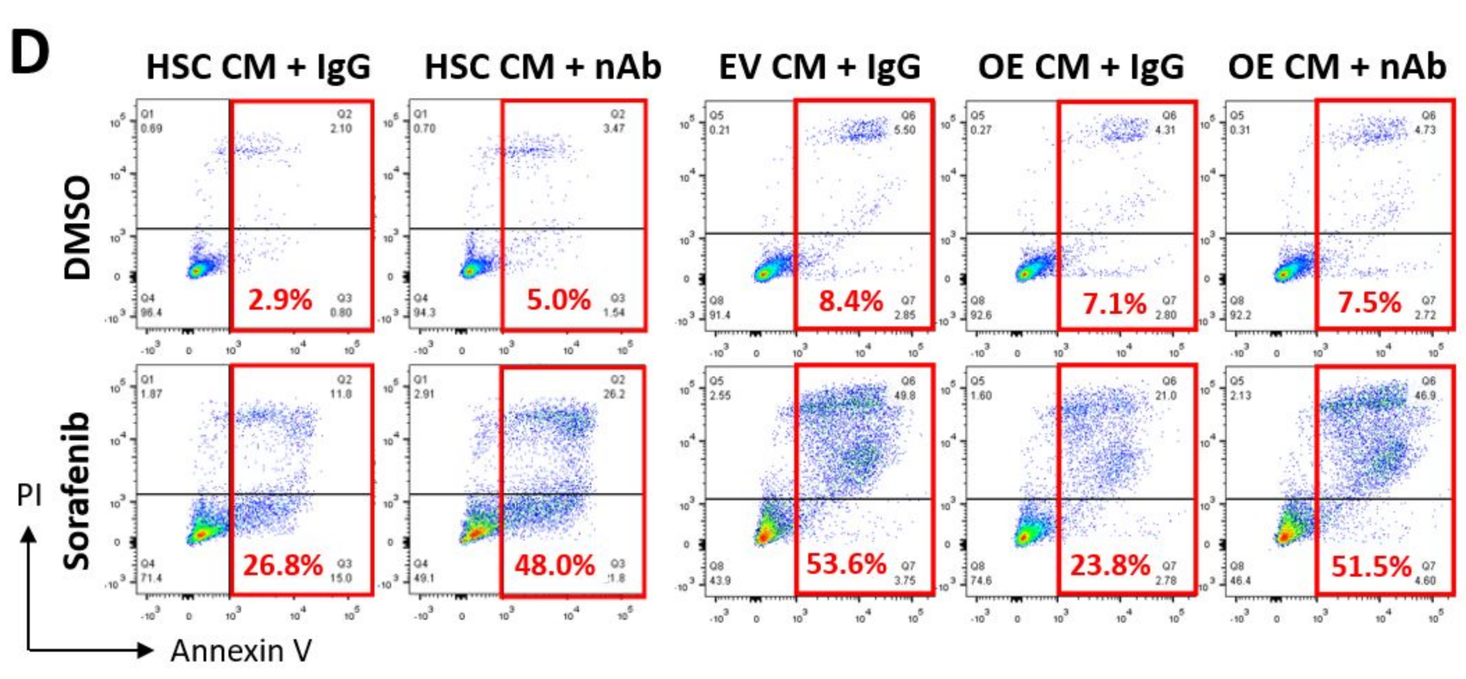

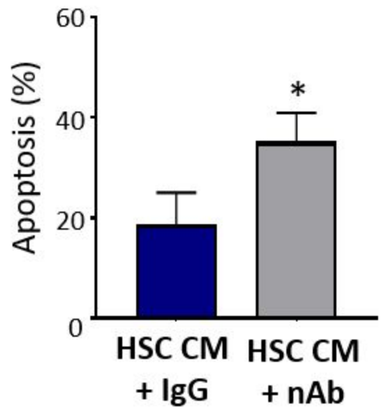

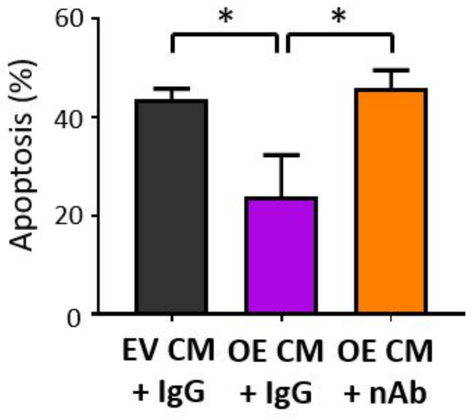

E

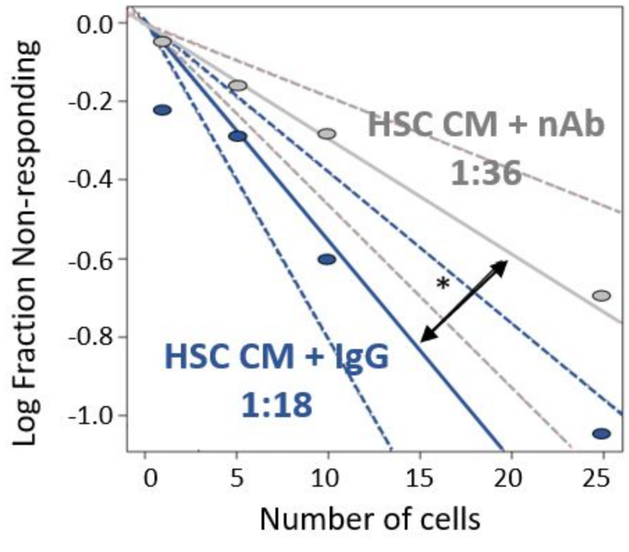

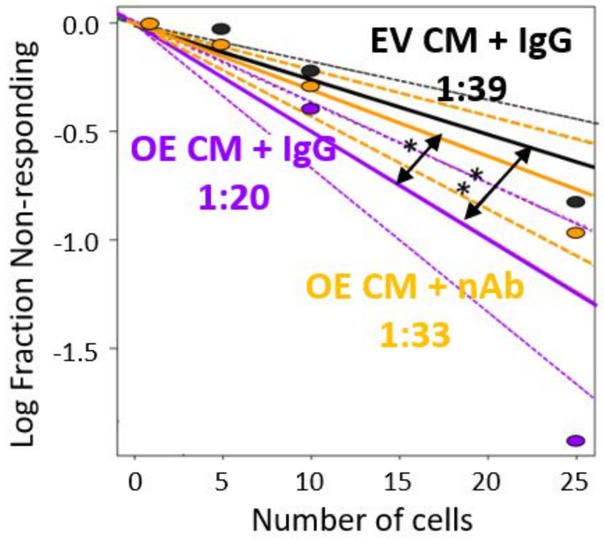

Loh JJ et al. Figure 3

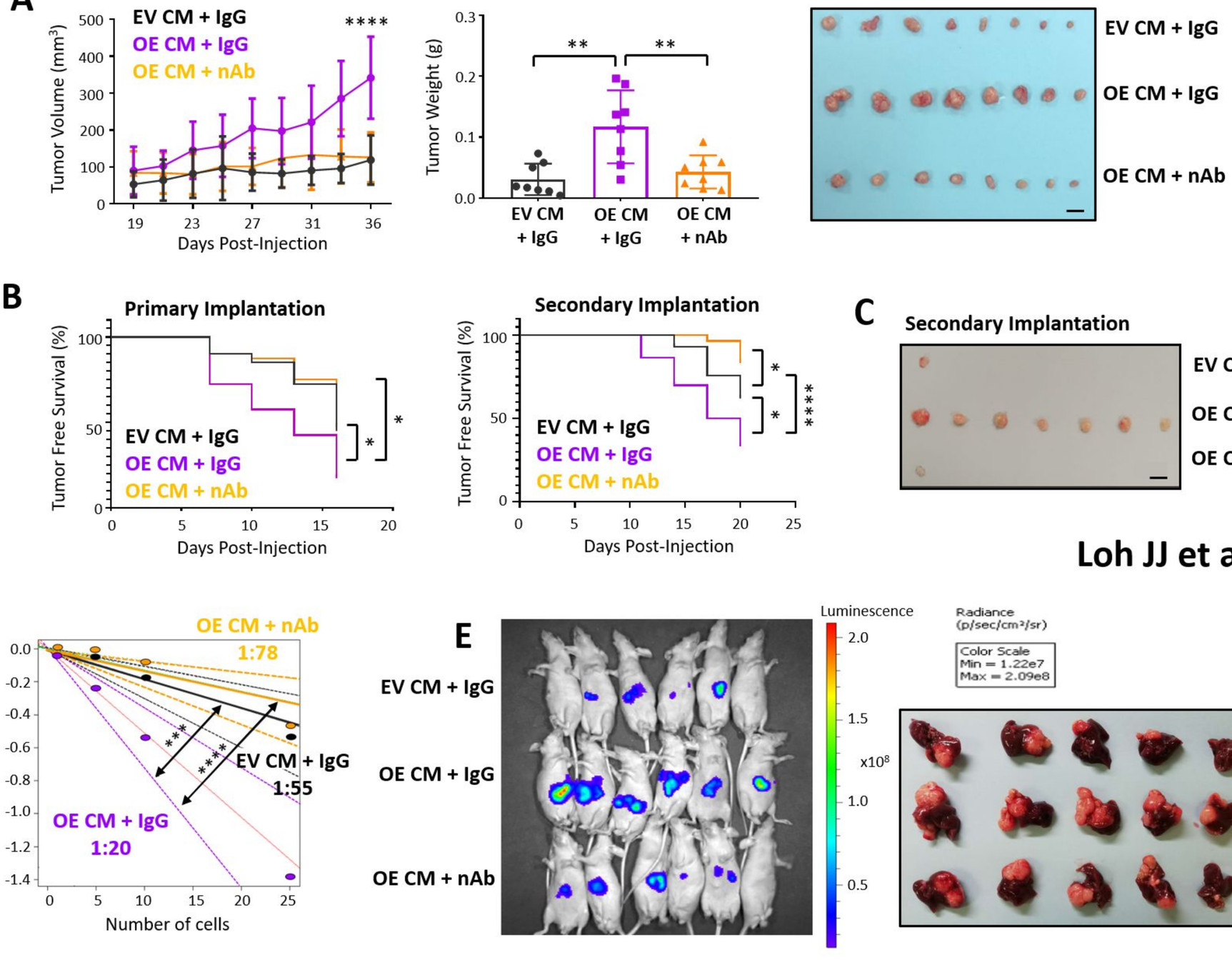

Loh JJ et al. Figure 4

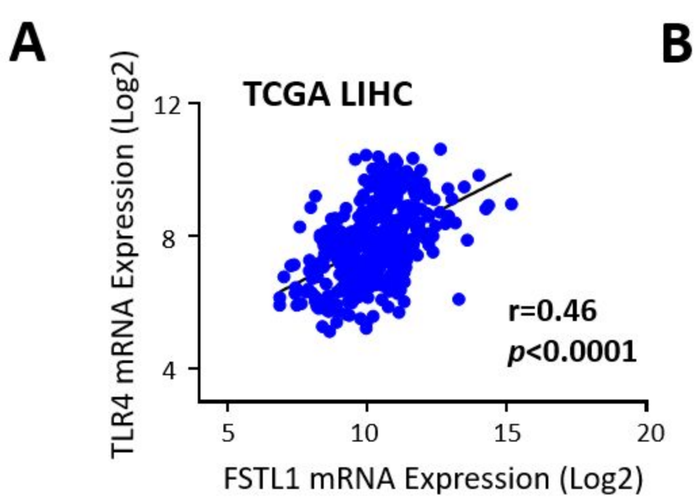

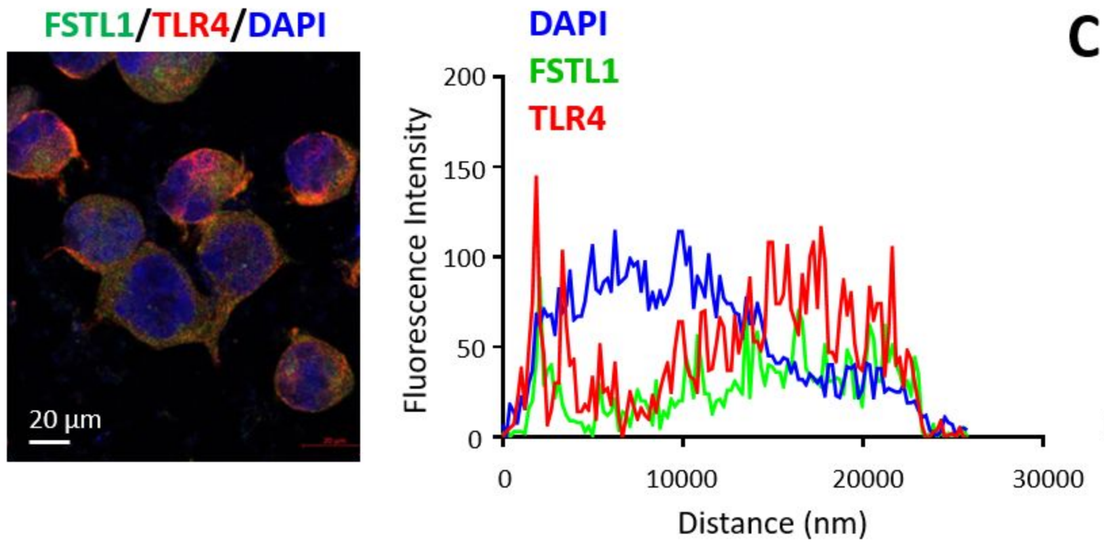

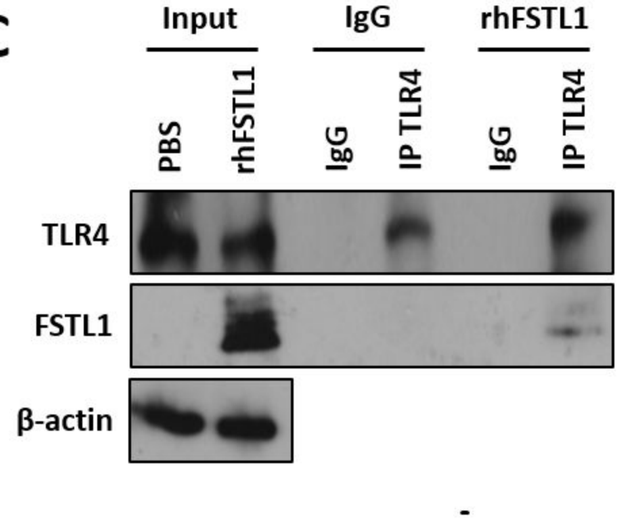

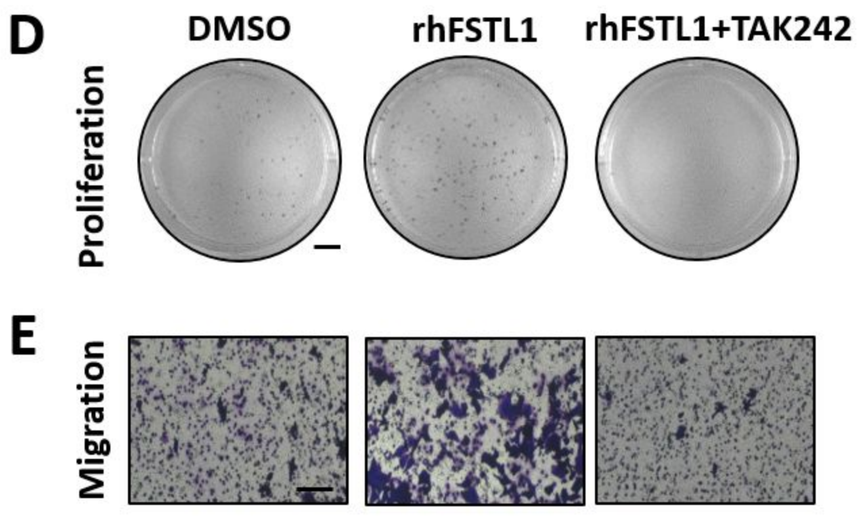

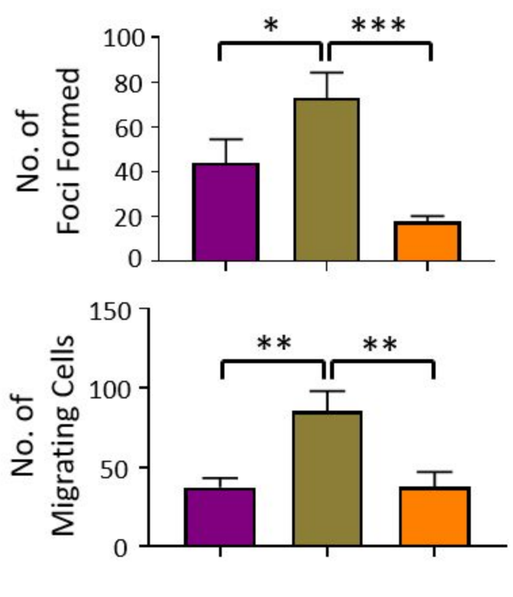

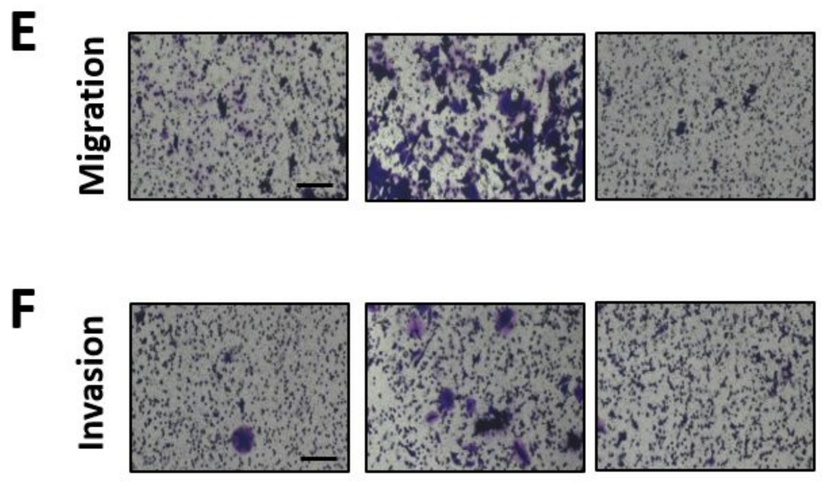

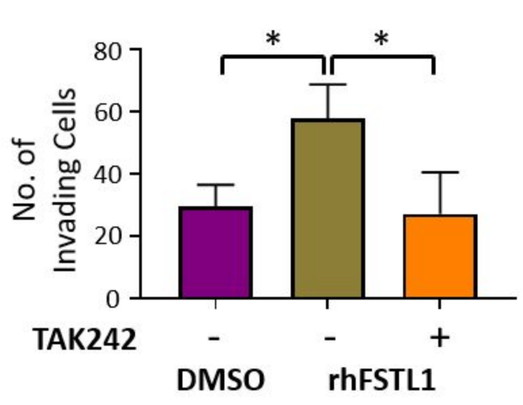

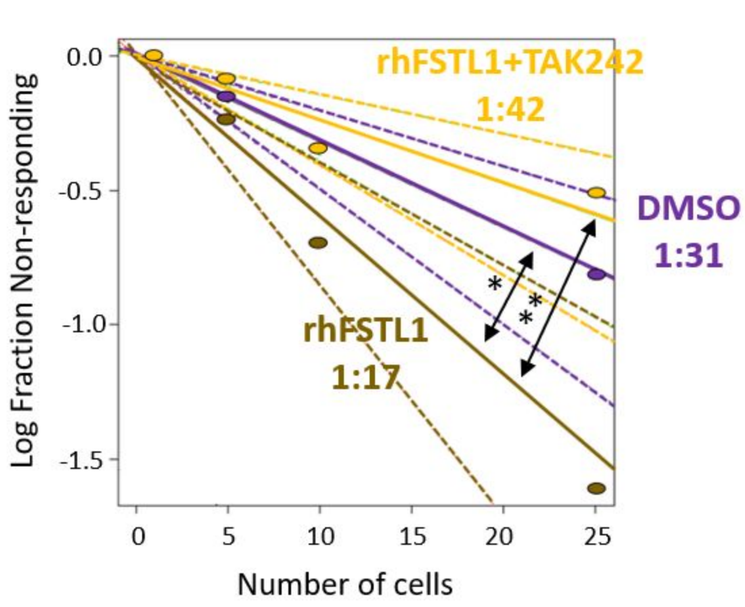

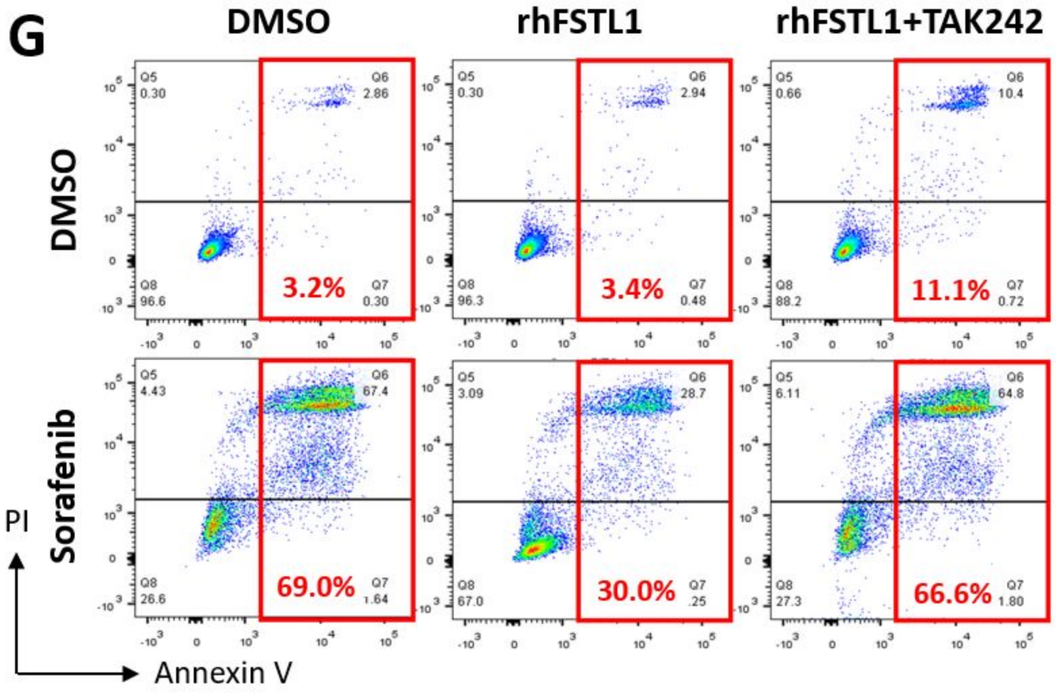

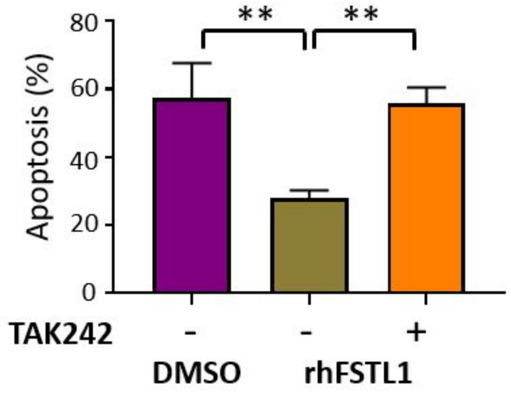

Loh JJ et al. Figure 5

Loh JJ et al. Figure 6

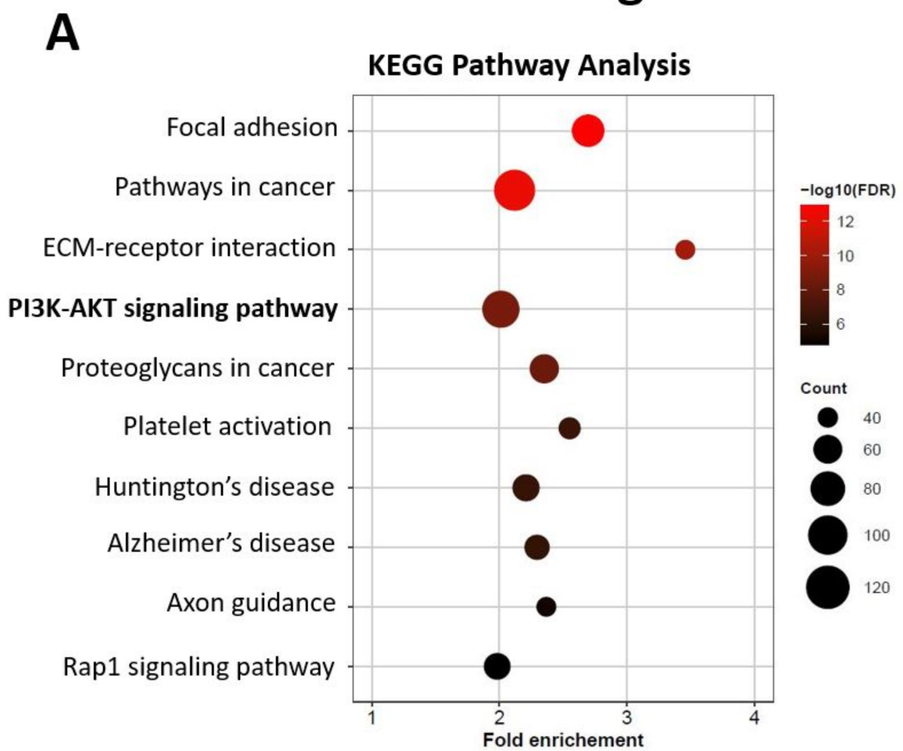

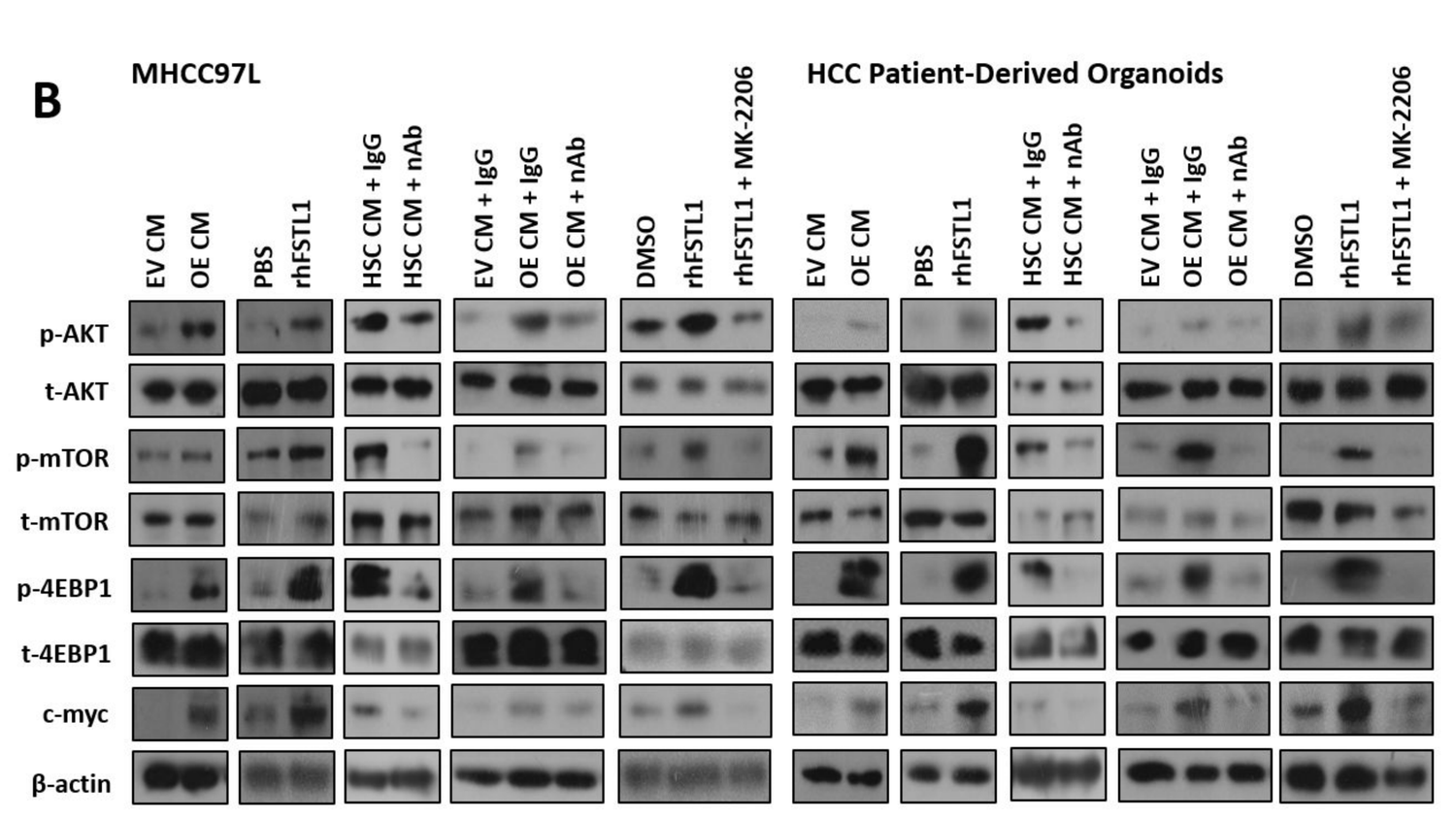

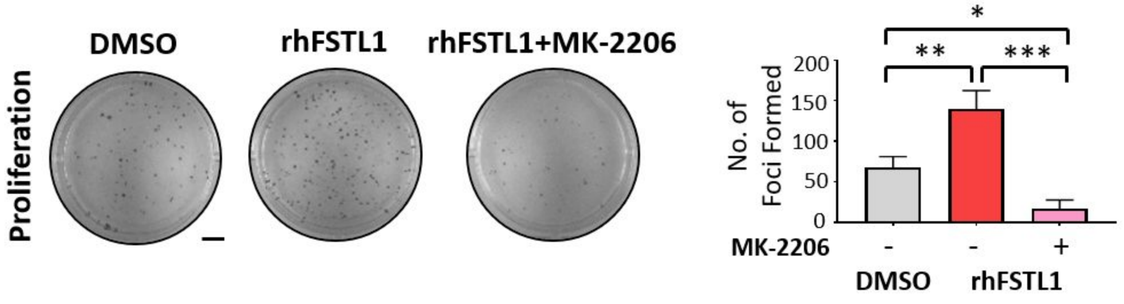

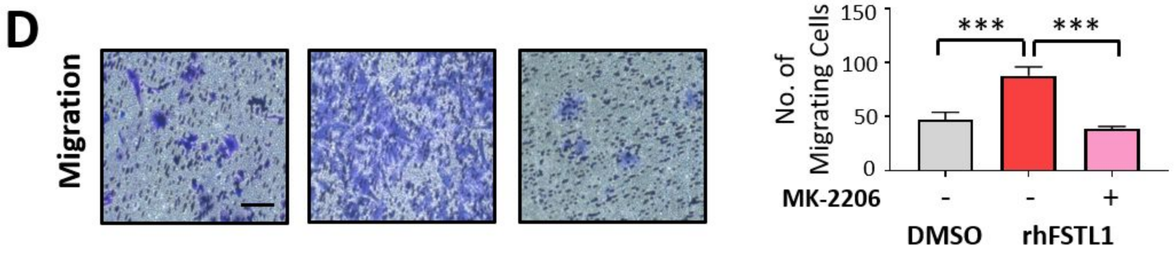

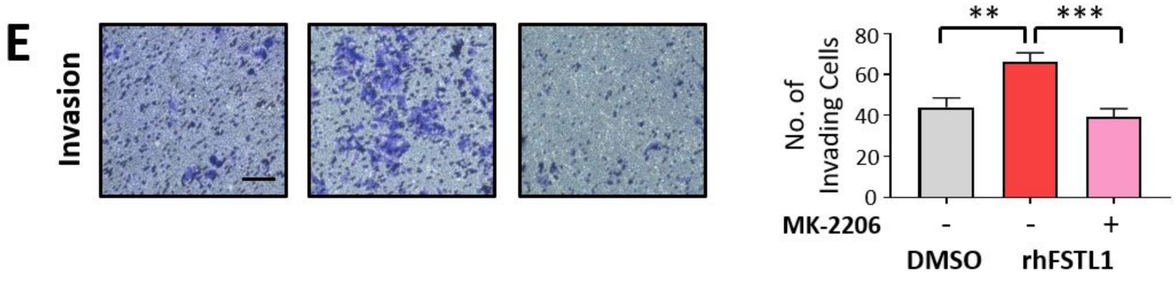

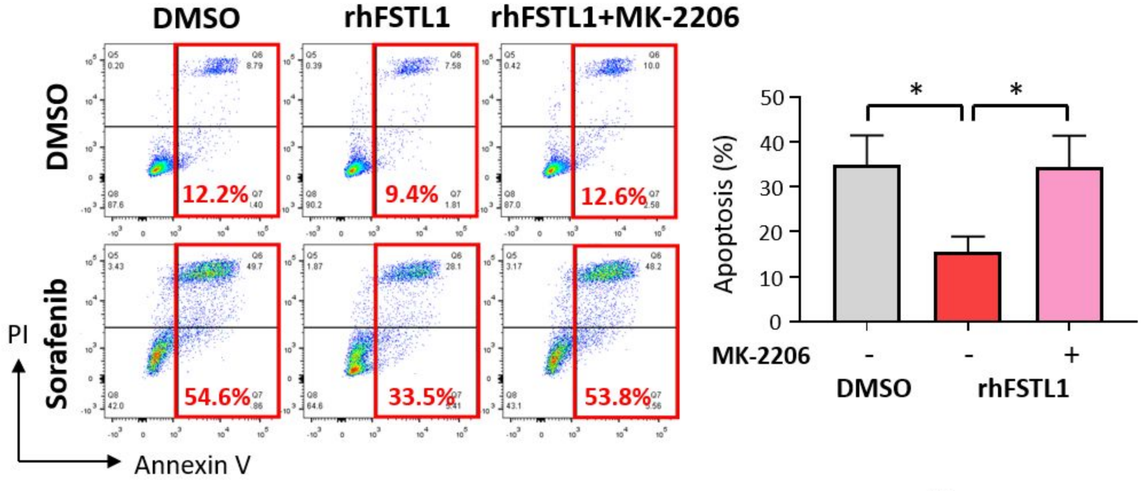

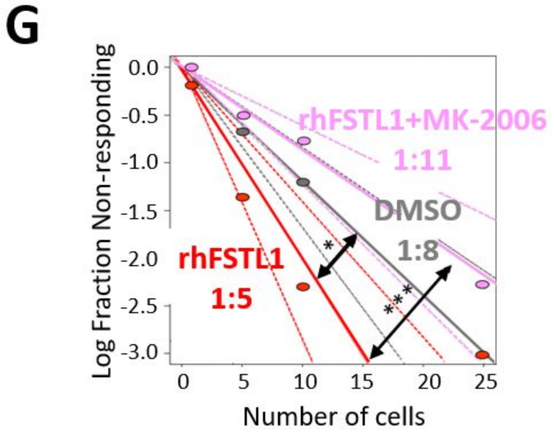

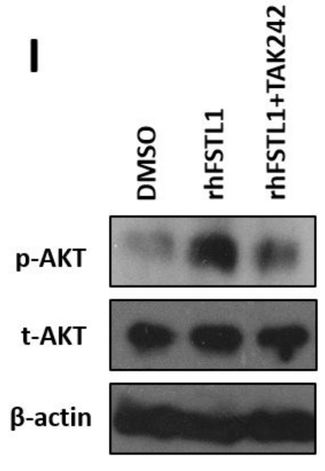

Loh JJ et al. Figure 7